NAVAL POSTGRADUATE SCHOOL

MONTEREY, CALIFORNIA

THESIS

EVOLUTION OF BOUNDARY LAYER HEIGHT IN RESPONSE TO SURFACE AND MESOSCALE FORCING

by

Matthew J. Moore

March 2005

Thesis Advisor:	Qing Wang
Second Reader:	Wendell A. Nuss

Approved for public release; distribution is unlimited

THIS PAGE INTENTIONALLY LEFT BLANK

REPORT DOCUMENTATION PAGE			Form Approved OMB No. 0704-0188
Public reporting burden for this collection of information is estimated to average 1 hour per response, including the time for reviewing instruction, searching existing data sources, gathering and maintaining the data needed, and completing and reviewing the collection of information. Send comments regarding this burden estimate or any other aspect of this collection of information, including suggestions for reducing this burden, to Washington headquarters Services, Directorate for Information Operations and Reports, 1215 Jefferson Davis Highway, Suite 1204, Arlington, VA 22202-4302, and to the Office of Management and Budget, Paperwork Reduction Project (0704-0188) Washington DC 20503.			
1. AGENCY USE ONLY	**2. REPORT DATE** March 2005	**3. REPORT TYPE AND DATES COVERED** Master's Thesis	
4. TITLE AND SUBTITLE Evolution of Boundary Layer Height in Response to Surface and Mesoscale Forcing			**5. FUNDING NUMBERS**
6. AUTHOR(S) Matthew J. Moore			
7. PERFORMING ORGANIZATION NAME(S) AND ADDRESS(ES) Naval Postgraduate School Monterey, CA 93943-5000			**8. PERFORMING ORGANIZATION REPORT NUMBER**
9. SPONSORING /MONITORING AGENCY NAME(S) AND ADDRESS(ES) N/A			**10. SPONSORING/MONITORING AGENCY REPORT NUMBER**
11. SUPPLEMENTARY NOTES The views expressed in this thesis are those of the author and do not reflect the official policy or position of the Department of Defense or the U.S. Government.			
12a. DISTRIBUTION / AVAILABILITY STATEMENT Approved for public release; distribution is unlimited.			**12b. DISTRIBUTION CODE**

13. ABSTRACT (maximum 200 words)

This thesis study focuses on understanding the dissipation processes of the stratocumulus deck after sunrise. This objective is met through careful analyses of observational data as well as model simulations. Measurements from the Marine Atmosphere Measurement Lab (MAML) of the Naval Postgraduate School (NPS) are used in this study. In particular, the half-hourly wind profiler/Radio Acoustic Sounding System (RASS) measurements were used to determine the boundary layer top and the evolution of the boundary layer mean thermodynamic properties during the cloud breakup period. Measurements from a laser ceilometer and the routine surface measurements are also used to detect the variation of cloud base height, the evolution of the cloud deck, and the onset of sea breeze. These measurements revealed the increase of the boundary layer depth after sunrise followed by a decrease of the boundary layer depth after the onset of the sea breeze, which points to the role of surface heating and sea breeze development in modulating cloud evolution. The effects of surface heating and sea breeze are further tested using a 1-dimensional mixed layer model modified for coastal land surfaces.

14. SUBJECT TERMS : Marine Atmosphere Measurement Lab (MAML), Wind profiler/Radio Acoustic Sounding System (RASS), boundary layer depth, mixed layer model	**15. NUMBER OF PAGES** 75
	16. PRICE CODE

17. SECURITY CLASSIFICATION OF REPORT	**18. SECURITY CLASSIFICATION OF THIS PAGE**	**19. SECURITY CLASSIFICATION OF ABSTRACT**	**20. LIMITATION OF ABSTRACT**
Unclassified	Unclassified	Unclassified	UL

NSN 7540-01-280-5500

Standard Form 298 (Rev. 2-89)
Prescribed by ANSI Std. 239-18

THIS PAGE INTENTIONALLY LEFT BLANK

Approved for public release; distribution is unlimited

EVOLUTION OF BOUNDARY LAYER HEIGHT IN RESPONSE TO SURFACE AND MESOSCALE FORCING

Matthew J. Moore
Lieutenant Commander, United States Navy
B.S., Southern Illinois University, 1991
M.S.A., Central Michigan University, 1993

Submitted in partial fulfillment of the
requirements for the degree of

MASTER OF SCIENCE IN METEOROLOGY AND PHYSICAL OCEANOGRAPHY

from the

NAVAL POSTGRADUATE SCHOOL
March 2005

Author: Matthew J. Moore

Approved by: Qing Wang
Thesis Advisor

Wendell A. Nuss
Second Reader

Philip A. Durkee
Chairman, Department of Meteorology

THIS PAGE INTENTIONALLY LEFT BLANK

ABSTRACT

This thesis study focuses on understanding the dissipation processes of the stratocumulus deck after sunrise. This objective is met through careful analyses of observational data as well as model simulations. Measurements from the Marine Atmosphere Measurement Lab (MAML) of the Naval Postgraduate School (NPS) are used in this study. In particular, the half-hourly wind profiler/Radio Acoustic Sounding System (RASS) measurements were used to determine the boundary layer top and the evolution of the boundary layer mean thermodynamic properties during the cloud breakup period. Measurements from a laser ceilometer and the routine surface measurements are also used to detect the variation of cloud base height, the evolution of the cloud deck, and the onset of a sea breeze circulation. These measurements revealed the increase of the boundary layer depth after sunrise followed by a decrease of the boundary layer depth after the onset of the sea breeze, which points to the role of surface heating and sea breeze development in modulating cloud evolution. The effects of surface heating and sea breeze are further tested using a 1-dimensional mixed layer model modified for coastal land surfaces.

THIS PAGE INTENTIONALLY LEFT BLANK

TABLE OF CONTENTS

THIS PAGE INTENTIONALLY LEFT BLANK

LIST OF FIGURES

LIST OF TABLES

THIS PAGE INTENTIONALLY LEFT BLANK

ACKNOWLEDGMENTS

I would like to thank my advisor, Dr. Qing Wang, of the Department of Meteorology, Naval Postgraduate School, for her guidance and support during the development of this thesis. Additionally, I would like to thank Dr. Wendell Nuss for his helpful comments as the second reader. Also, thank you to Mr. Dick Lind for his direct contribution in providing me with the data for this study and Dr. John Kalegiros for helping with the profiler data processing. I would also like to acknowledge the support of my friends and classmates: Tom Moneymaker, Sim James, Justin Reeves, Matt Lear and Al Semedo.

Finally, and most importantly, the loving support from my wife, Carrie, and children, Matthew, Nicholas and Melanie. They make everything possible.

THIS PAGE INTENTIONALLY LEFT BLANK

I. INTRODUCTION

The structure and evolution of the atmospheric boundary layer are of great meteorological interest and significant tactical importance to the United States Navy. Of particular interests is the stratocumulus-topped marine boundary layer, which is the focus of this thesis study. A stratocumulus layer adds a level of complexity and uncertainty in the ability to diagnose or predict the boundary layer structure due to the complicated cloud microphysics and radiation associated with the cloud layer and their interaction with the boundary layer dynamics. Consequently, large uncertainties exist in current model prediction systems when stratocumulus clouds are present, which adversely affect the effectiveness of tactical decisions. The presence of stratocumulus clouds significantly enhances the boundary layer inversion strength, which plays a primary role in Electromagnetic and Electro Optical propagation. Also, changes in inversion stability and strength may in turn modify cloud evolution. The resulting changes to cloud structure have a direct impact on military remote sensing and surveillance capabilities. Therefore, an improved understanding of the evolution of a stratocumulus-topped boundary layer would significantly contribute to the United States Navy's tactical exploitation of the environment.

Low cloud ceilings also affect human activities such as airport operations. Figure 1 shows the stratocumulus cloud deck that covers the entire northern California coast including the coastal land. In many cases, the cloud base may touch the ground, which is then categorized as fog. For major airports such as San Francisco International Airport, early breakup of the cloud layer means an increased number of landings and take-offs of commercial airplanes and less delays. However, one needs to understand the mechanisms of cloud breakup in the near-coast region in order to correctly represent them in prediction models for accurate forecasts of the cloud break up.

The Radar Wind Profiler (RWP) and Radio Acoustic Sounding System (RASS) has become an important tool in both research and operational meteorology. Complex forecasting problems such as forecasting fog and coastally trapped disturbances (CTDs) have been made easier through the use of a RWP (Ralph et al., 1997). Wang et al. (1999) suggested that the profiler/RASS system can be used to define the marine boundary layer

height. Although the vertical resolution of profiler/RASS system is relatively coarse, it provides a continuous measurement of the low-level wind and temperature profiles which allows us to obtain statistically significant results from large datasets from the profiler/RASS.

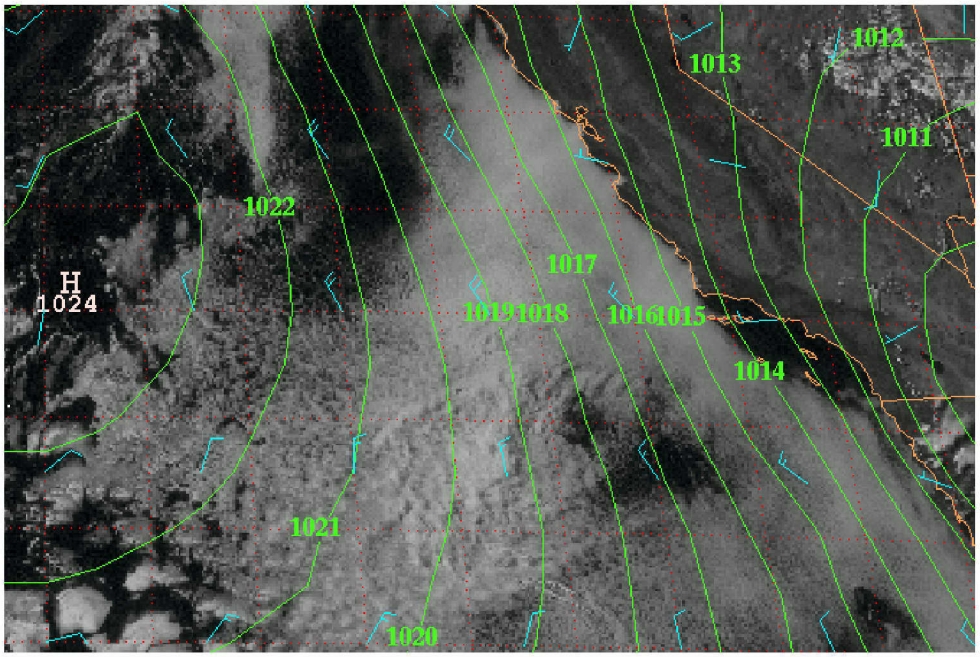

Figure 1. Visible satellite image on 11Aug 2004. The fog layer over the San Francisco International and Monterey airports is seen in this image. The solid green lines show contours of surface pressure in mb.

The objective of this thesis is to understand the evolution of the Marine Boundary Layer along the California coast with a focus on the early morning transition from a stratocumulus-topped boundary layer to a clear boundary layer. The dissipation of the morning stratocumulus clouds is usually referred to as the cloud 'burn-off'. This objective is achieved through a combination of data analysis and numerical simulations. Measurements at the NPS Marine Atmospheric Measurement Laboratory (MAML), including a profiler/RASS system, a laser ceilometer, and other routine surface meteorological variables are used. A 1-dimensional moist mixed layer model will also be used to assist in understanding the cloud break up mechanisms. The measurements and statistical analysis of the suite of ground-based measurements will help to quantify the diurnal characteristics of the MBL. Chapter II includes a discussion of the general

characteristics of the inversion off California. Chapter III discusses the instrumentation and data. Chapter IV provides the method and results from data analysis. Chapter V includes model simulation and discussion. Finally, Chapter VI gives conclusions and recommendations for further study.

THIS PAGE INTENTIONALLY LEFT BLANK

II. GENERAL CHARACTERISTICS OF THE MARINE ATMOSPHERIC BOUNDARY LAYERS

A. PHYSICAL PROCESSES IN THE STRATOCUMULUS-TOPPED BOUNDARY LAYERS

The Stratocumulus-topped (STCU) boundary layer is a major phenomenon of the west coast of California. This type of boundary layer occurs mostly on the west coast of major continents in subtropical latitudes where large-scale subsidence occurs over cool upwelling water (Hanson 1991). The following diagram (Whisenhant, 1999) depicts the major physical processes in STCU boundary layers. Here, radiative cooling at the

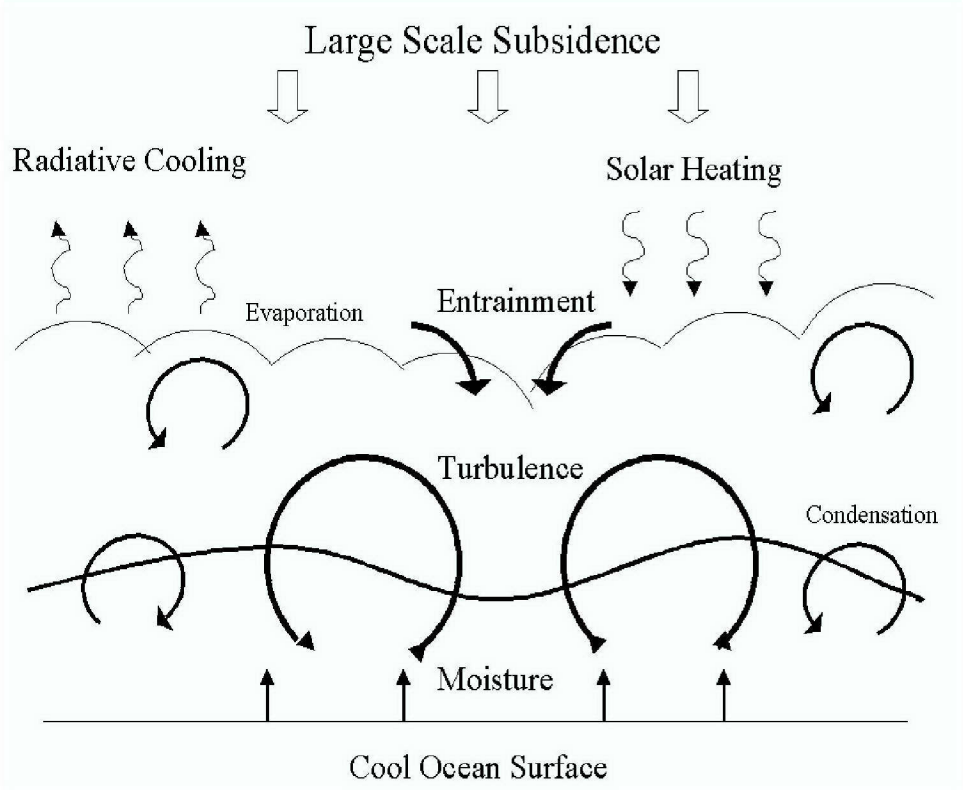

Figure 2. Physical processes occurring in STCU boundary layers (from Whisenhant, 1999).

cloud top is the main source of turbulent mixing within the boundary layer although shear and surface buoyancy flux may also contribute. Because of the low sea surface temperature (SST) due to coastal upwelling, surface buoyancy flux is usually small, on the order of 10 Wm^{-2} or less and is sometimes negative.

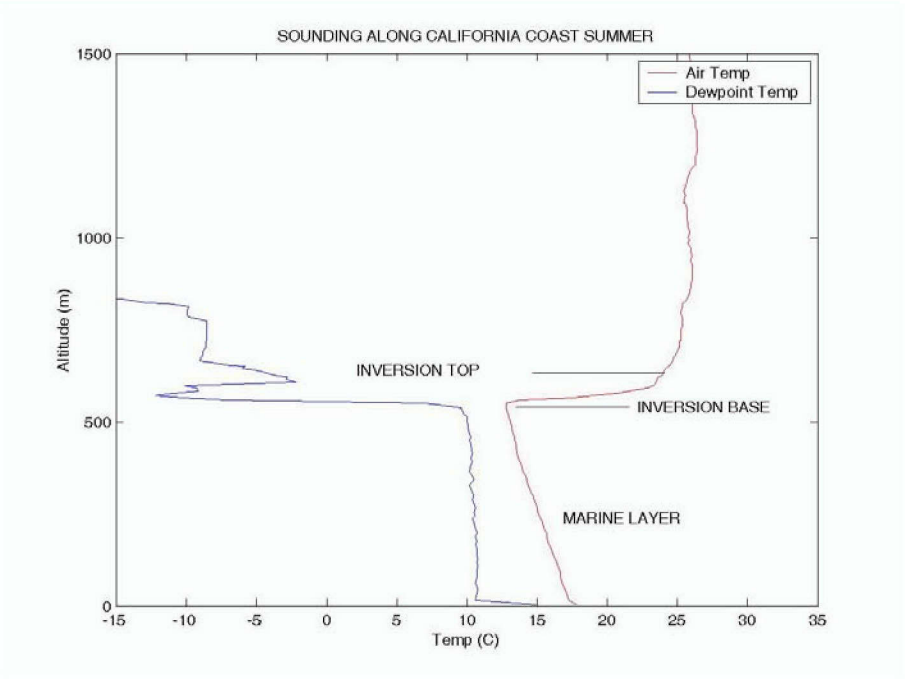

Figure 3. A typical sounding through the summertime stratocumulus-topped boundary layer in the California coast.

Figure 3 shows the typical vertical variation of temperature and water vapor in a STCU boundary layer. Immediately above the boundary layer, the atmosphere is characterized by a strong temperature and water vapor gradient in a very shallow layer on the order of 20 m, which is usually referred to as the capping inversion. The inversion is formed by a combination of subsidence, or sinking of air, produced by the Eastern Pacific High (EPH), and turbulent mixing over the cool Eastern Pacific waters. The depth and vertical gradients of the inversion are influenced by many factors, including a synoptic scale divergence field and coastal effects such as sea breezes and coastal jets.

In the summer, the EPH is very strong, around 1020-1030 hPa and is positioned further north. This increases the subsidence and thus, the adiabatic warming aloft. A strong northwesterly wind results from this unique synoptic weather pattern. This northwesterly wind causes the upper layer of water along the coast of California to be

transported offshore. This water is then replaced by up welled water from below which is much cooler than the water it replaced. This combination of increased subsidence and upwelling along the coast creates an inversion that is generally much stronger in the summer time. This strong inversion traps cool, moist air close to the surface, which is the reason why much of the California coastline is blanketed by a thick stratus or fog layer for many hours each day in the summer.

The inversion atop the MBL is much weaker in the winter months. Subsidence is not as strong since the EPH is further south, and the air sea temperature difference is much less. This is because there is a lack of upwelling and the air is much cooler. The synoptic pattern is more variable as mid-latitude cyclones transit this region in the wintertime. As a result the inversion is a much different phenomenon to study in the winter season. This study will focus on the summer months of June and July.

Diurnal variation of stratocumulus (STCU) clouds has long been documented in the literature (e.g., Betts, 1990). This variation is characterized by an increased cloud depth at night and a decrease during the day, which is accompanied with a daytime increase of the cloud base height and decoupling of the daytime cloudy boundary layer. Various modeling studies (Turton and Nichols 1987, for example) have suggested differential solar warming as the cause of this diurnal variation. This happens when the short-wave radiation warms the cloud layer more than the below-cloud layer. This differential heating stabilizes the region near the cloud base and results in decoupling of the entire boundary layer, which cuts off the moisture supply from the ocean surface to the cloud layer and eventually leads to cloud breakup during the day (Wang et al., 1999).

Similar diurnal variations of STCU were also observed through ground-based observations over San Nicolas Island off the coast of Southern California (Blaskovic and Davis 1991). Although the island effects were considered minimal so that the observed diurnal variations were considered to be those of typical marine stratocumulus, the surface air temperature was found to have strong diurnal variation as well with a diurnal range of 2°C.

B. DIURNAL VARIATION OF STCU BOUNDARY LAYER OVER COASTAL LAND

One major characteristic of the coastal STCU is the strong diurnal variation of cloud penetration into coastal land surfaces. This variation includes the onset of cloud cover in the afternoon and the morning breakup of STCU (the so-called morning burn-off). This diurnal variation is also accompanied by variations in cloud thickness and drizzle precipitation. Visible satellite images show that the coastal STCU is sometimes well connected to the extensive STCU cover over the open ocean, but it is also observed to be independent of the STCU off the coast. Accurate prediction of cloud breakup near the coast is crucial for various human activities, but is currently poorly forecast with existing regional models. The nature of cloud formation and dissipation at the coast has received little attention and is the least understood coastal phenomenon.

The climatology of the coastal region is complicated by a variety of mesoscale circulations, particularly during the summer. On the West Coast, mesoscale circulation can be characterized into two categories: thermally driven circulation and orographically forced disturbances. These flow fields interact with the marine boundary layer and regulate the variation of boundary layer height along and across the coast. Since the marine boundary layer is generally moisture rich and the marine layer off the coast is often covered by STCU, the coastal circulations/disturbances are usually associated with the advection/formation of STCU. For example, STCU was found to be associated with the coastally trapped events that propagate northward along the coast (Dorman, 1985).

One of the most significant mesoscale features of the summer-time coastal zone is the thermal circulation associated with the land-sea thermal contrast. While the basic structure of the sea breeze circulation has been known for a long time, significant advances were made over the past ten years in understanding some of the important aspects of this phenomenon. This is particularly true in the Monterey Bay area, where several intensive observational periods have been made in the past ten years. Banta et al. (1993) found that the sea breeze component in the Monterey Bay area was in general perpendicular to the coastline and that there were two different time and length scales in the sea breeze circulation in an offshore large scale environment. The inner circulation started in the morning between 0900 PST and 1000 PST. This circulation was shallow (a

depth of 300 m), less intense, and had a horizontal scale of 30 to 40 km. The outer circulation started at noon and had a horizontal scale of 100 km. This circulation was related to the large-scale thermal difference between the land and sea.

In addition, coastal flow plays a significant role in modifying the large-scale subsidence and regulates the variation of boundary layer height in addition to modifying the low-level wind shear. These factors change the nature and intensity of turbulent kinetic energy and affect the evolution of SC through cloud-top entrainment. Their role in STCU evolution should be examined as well.

One of the important stages of the diurnal variation of coastal STCU is the morning dissipation of STCU, the so-called cloud burn-off. Burn-off occurs in the morning a few hours after sunrise. The process is apparently associated with solar radiation. However, solar radiative flux affects cloud evolution in several different ways. Over the water, it causes decoupling of the boundary layer cutoff the moisture supply into the cloud layer. Over the coastal land, the surface heat flux increase after sunrise may a play major role in modifying boundary layer dynamics, but we still do not have a quantitative understanding of its effects.

C. THE SCOPE OF THIS RESEARCH

Although there are many issues with the STCU boundary layer near the coast, this thesis research limits its scope to quantifying and understanding the processes affecting the day-time clearing of the cloud layer over the coastal land surfaces. Related to the cloud clearing, we will also study the characteristics of sea breeze onset near Marina, CA. The primary dataset used for this study is the wind and temperature profiles from a profiler/RASS maintained by the Meteorology Department of the Naval Postgraduate School, Monterey, CA. We particularly focused on measurements in the summer months of June and July of 1999 through 2003. This dataset is also augmented by the ground-based routine meteorological measurements (mean temperature, relative humidity, wind, and upward looking solar and infrared radiation). Measurements from a laser ceilometer were also used to determine the variation of the cloud base.

THIS PAGE INTENTIONALLY LEFT BLANK

III. INSTRUMENTATION AND DATA

The Meteorology Department of the Naval Postgraduate School maintains the Marine Atmospheric Measurement Lab (MAML) of the Meteorology Department located at 36.69^0 N latitude and 121.76^0 W longitude, just north of Marina's municipal airport. The ground level at the MAML is 51 m above sea level and about 5 km inland from the shoreline. The suite of instruments includes a profiler/RASS wind and temperature sounding system, surface meteorological measurements (pressure, temperature, relative humidity, and solar and infrared radiation), and a laser ceilometer. The profiler/RASS system operates continuously at 2 kHz acoustic frequency with measurements every 30 min. The laser ceilometer recorded cloud base height, at 1 min averages. Surface measurements of temperature, pressure, relative humidity, and downward solar and infrared radiation were recorded as 2 minutes averages. These measurements are made continuously throughout the year. Measurements from all these components were used for this study.

A. RADAR WIND PROFILER AND RADIO ACOUSTIC SOUNDER SYSTEM

Radar Wind Profilers are specifically designed to measure vertical profiles of horizontal wind speed and direction from near the surface to above the tropopause depending on the frequency (NOAA 2005). Figure 4 shows the 915 MHz profiler/RASS site at Fort Ord.

Figure 4. NPS 915 MHz Profiler/RASS system at MAML.

The 915 MHz system is capable of retrieving wind measurements in the lower stratosphere every 5 minutes. The RASS system is also capable of measuring and producing vertical temperature profiles of the atmosphere through the use of sound waves. The radio frequency used by the RASS is 2000-2100 MHz or half the wavelength transmitted by the 915 MHz profiler signal (NOAA 2005). The RASS works through the use of Doppler temperature affects on the speed of sound. Thus variations in the speed of sound can be converted to a virtual temperature profile of the atmosphere. These virtual temperature profiles will be used is this study to measure the Atmospheric Boundary Layer.

The profiler/RASS measurements are used to characterize the vertical structure of the atmospheric boundary layer. Figure 5 shows on example of the vertical profiles. The virtual potential temperature (θ_v, Figure 5a) is derived from the RASS virtual temperature using the pressure obtained from the met tower and assuming a hydrostatic balance in the lower atmosphere. These profiles are used to identify the boundary layer height. This is done by identifying the inversion base from the soundings. In the example shown in Figure 5, we identify the boundary layer height to be 280 m. In some soundings, a strong wind shear can be observed close to the inversion.

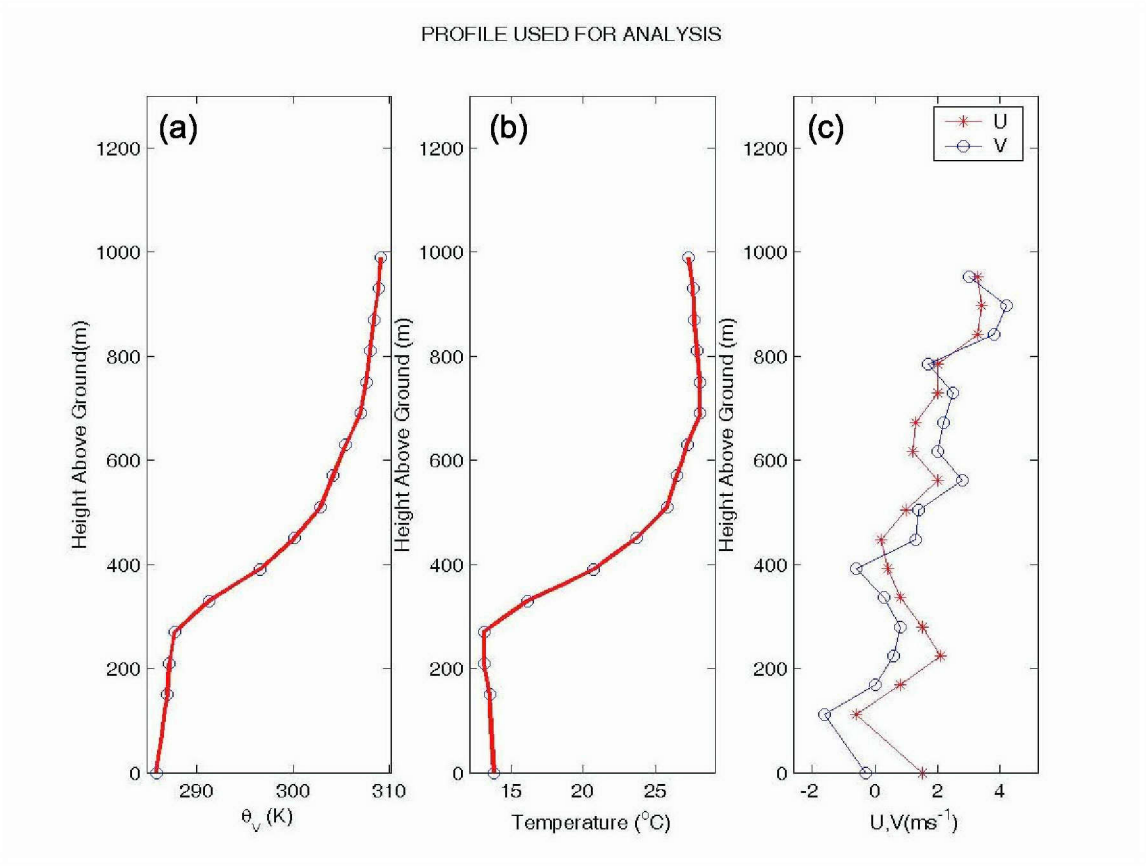

Figure 5. Vertical profiles of the lower atmosphere from the profiler/RASS measurements. (a) Virtual potential temperature, θ_v; (b) virtual temperature directly from the RASS measurements; and (c) Horizontal wind components.

B. SURFACE OBSERVATIONS

Surface observations of pressure, temperature, relative humidity, wind and radiation were made by the respective instrumentation, all mounted on the NPS surface met tower standing next to the profiler/RASS unit.

Figure 6. Fort Ord Surface met tower

Figure 7 shows the variation of all measured variables from the surface met tower during a 24 hour period.

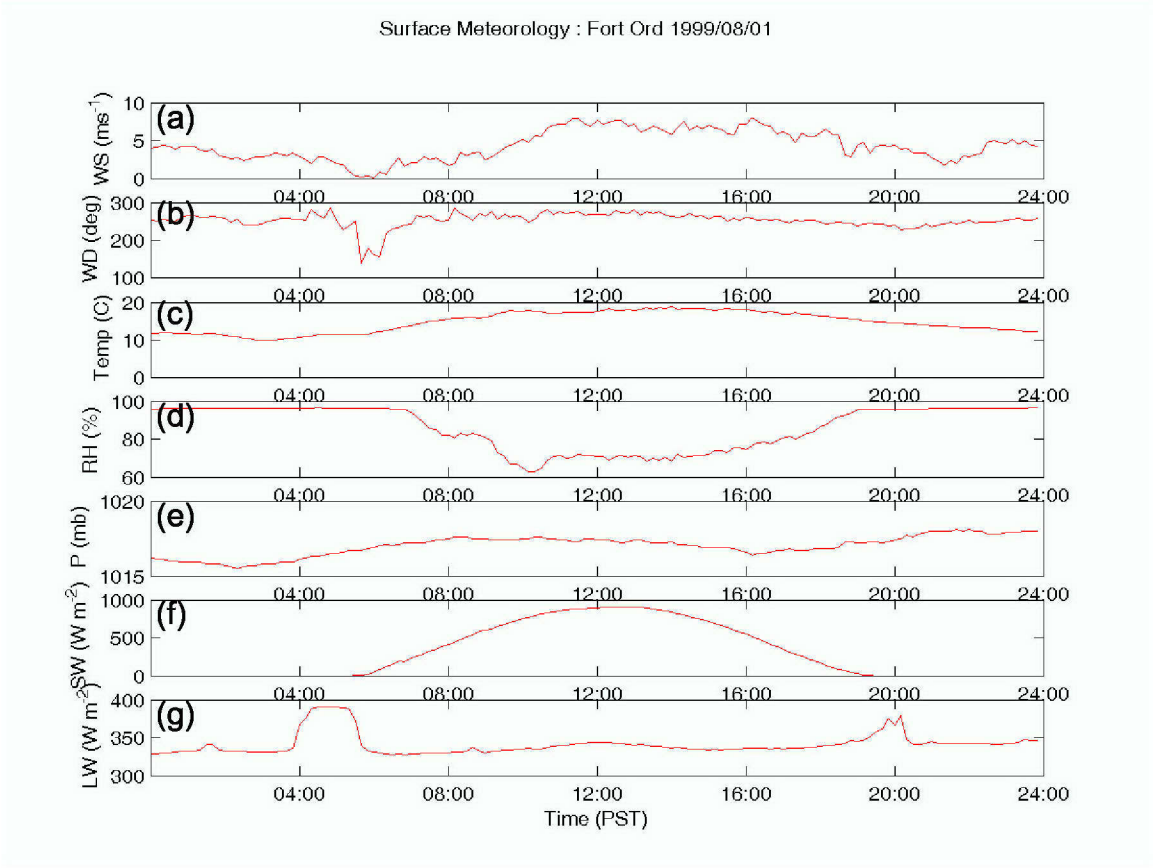

Figure 7. Time variation of the surface meteorological variables measured at MAML on August 1, 1999. (a) wind speed (ms^{-1}); (b) wind direction (degrees); (c) temperature (^{o}C); (d) relative humidity (%); (e) pressure (mb); (f) short wave downward radiative flux ($W\ m^{-2}$); and (g) longwave radiation ($W\ m^{-2}$).

Measurements were made on mostly cloudy day as detected in the variation of short and long-wave radiation (Figure 7f and 7g). In this study, we use the variation of these two variables to diagnose the presence of low-level stratocumulus cloud coverage that increases the downward longwave radiation and decreases the incoming solar radiation. A discontinuity is normally observed at the transition between cloudy and clear conditions. The wind speed (Figure 7a) shows an increase of wind speed in the early morning and the maximum wind is reached close to noon. This increase of wind speed was observed in many of the days we examined and considered as the impact of the sea breeze circulation as the background wind direction is nearly across the shore. We

thus use this signature to determine the onset of a sea breeze at the measurement location. Figures 7c and 7d also depict the warming and drying of the lower boundary layer in response to the solar heating.

C. LASER CEILOMETER

The CT25K laser ceilometer is a new generation general purpose cloud height sensor employing LIDAR technology for detection of clouds and aerosol-laden layers. The measurement range of the CT25K extends up to 25,000 feet (7.5 km) covering most heights where dense clouds appear. The instrument is capable of reporting up to three cloud layers simultaneously (ARM 2005). We used only the lowest cloud height for this study. It detects the cloud base reliably in fog, rain, snow and haze. If the cloud base is obscured, it measures and reports the vertical visibility. The CT25K is used as a stand-alone system or it can be integrated as a sensor in a meteorological system (ARM 2005). Figure 8 below shows the CT25K laser ceilometer.

Figure 8. The CT25K laser ceilometer

The ceilometer was used primarily in this study to measure the cloud base height. Once the height of the cloud base is obtained it can be combined with the height of the top of the clouds to produce cloud thickness. These measurements are a crucial when determining the diurnal transition of the boundary layer.

THIS PAGE INTENTIONALLY LEFT BLANK

IV. DATA ANALYSIS AND METHODOLOGY

A. DEFINING THE BOUNDARY LAYER HEIGHT AND CLOUD DEPTH

The profiler/RASS measurements provide vertical profiles of temperature and wind speed and direction continuously every 30 minutes. Although the vertical resolution is relatively coarse (60 m), the continuous detection of the boundary layer structure is advantageous. To examine the accuracy when using the profiler/RASS measurements to detect the boundary layer height, a comparison between RASS potential temperature profiles and those from rawinsonde launches in close vicinity were made by Wang et al. (1999) and is shown in Figure 9. Figure 9 shows a rather consistent result from the RASS and the rawinsondes, although the RASS profiles have a vertical resolution of about 60 m. This comparison shows good confidence when using the RASS θ_v profiles to characterize the evolution of virtual potential temperature.

We examined all vertical profiles at 1 hour intervals for the months of June and July between 1999 and 2003, which contains 7320 soundings in 305 days. This large dataset is needed to ensure statistical significance of our analysis. From each sounding, we obtained the boundary layer height (BLH, defined as a sharp inversion base), temperature at the BLH, the top of the sharp inversion, and the temperature at the top of the inversion.

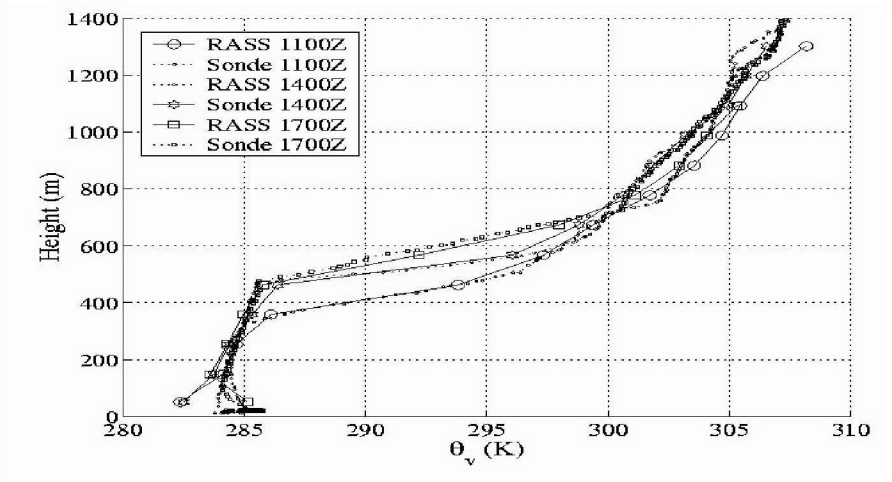

Figure 9. A comparison of vertical profiles of virtual potential temperature from RASS and from rawinsonde.

Combining the profile/RASS detected BLH and the cloud base measurements from the ceilometer, we are able to obtain the cloud depth. Since the ceilometer measurements were made at a different time interval and cloud bases at three levels may be detected, some filtering is needed to remove the higher cloud decks. Figure 10a shows the boundary layer and cloud base heights observed from June 4 to June 9 of 2003. This figure illustrates the strong diurnal variation of the cloud base, cloud top, and the cloud depth, respectively. In this Figure we can clearly see the boundary layer height rise through out the early part of the day, which is very typical of all the measurements we examined. However, we also notice that the boundary layer begins to decrease around local noon and the rapid decrease soon leads to cloud dissipation. In addition, the cloud base height also shows strong diurnal variation with a minimum cloud base height at night and a gradual increase in the early morning. A rapid increase of the cloud base height was also observed before the cloud break up. This can also be seen in the cloud depth in Figure 10b. Cloud depth in the early morning is about 500 m, as the day progresses it is evident that the cloud layer thins and dissipates. This transition occurs at about the same time every day. This increase in height of the boundary layer occurs during the early part of the day, about 3-5 hours after sunrise as expected.

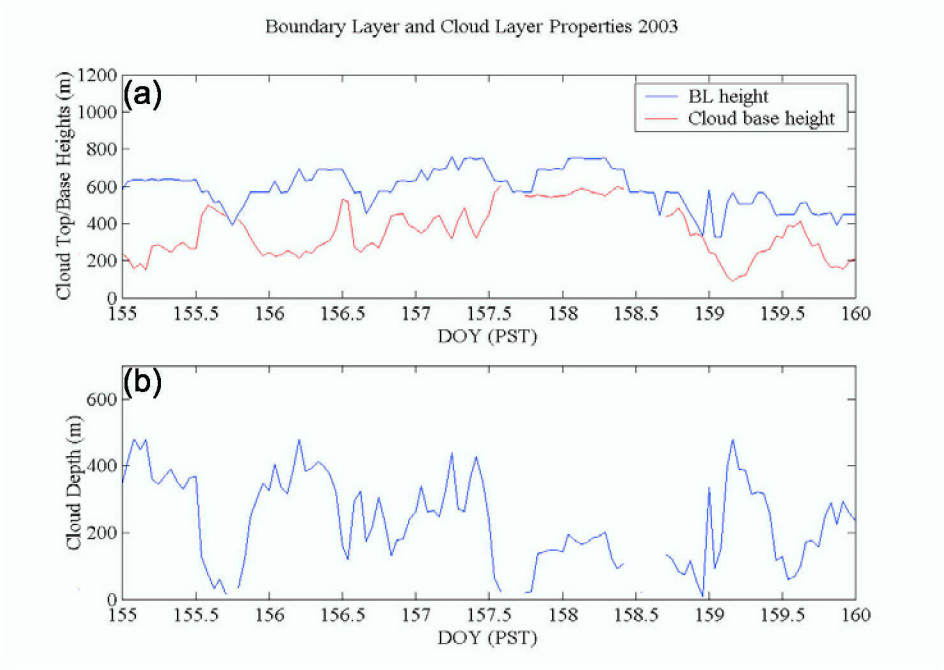

Figure 10. Diurnal variation of (a) BLH and cloud base height (m); and (b) cloud depth between June 4 and June 9 of 2003.

Wang et al. (1999) examined some vertical profiles from profiler/RASS system and identified the increase of BLH in the early morning. Their model simulation suggests the dominant effects of solar heating of the ground and the subsequent increase in surface heat flux. What was not expected was the decrease of the BLH just prior to cloud dissipation and it seems to speed up the cloudy-clear transition as shown in Figure 10. This simple graph clearly shows this phenomenon. This type of transition is evident through out the most of the data sets collected. This break-up is evidently associated with solar radiation. However, it is not clear how solar radiation resulted in this break-up. One theory is that the on-set and ramp-up of the sea breeze plays a roll in the cloud dissipation. This theory will be explored is this study.

B. DIAGNOSING CLOUDY/CLEAR CONDITIONS

To understand the characteristics of cloud evolution and its relationship with surface heating and local thermal circulation, we identified the cloud/clear condition for every hour during the period of measurements during this study. The cloudy/clear condition is identified from the time evolution of the mean meteorological variables for each local day using a combination of solar and infrared radiation measurements at the met tower at MAML. To begin we first looked into the diurnal variation of temperature, relative humidity, long and short wave radiation process along with the wind speed and direction observed from the suite of surface met instruments. Figure 11 is an example of the diurnal variation of all these variables.

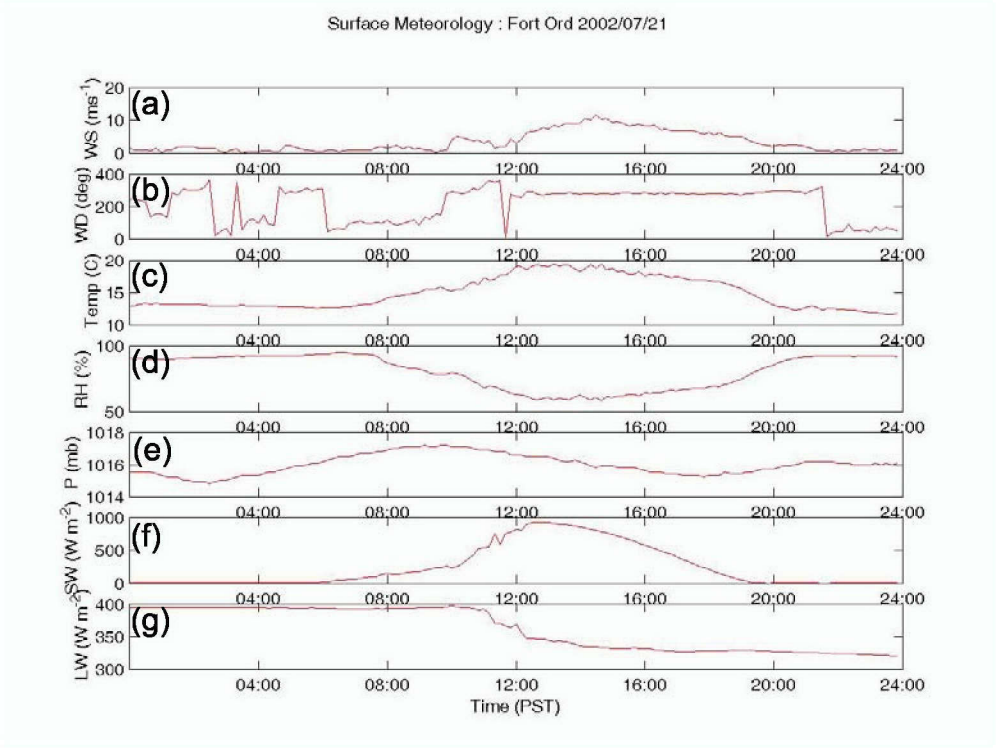

Figure 11. Same as in Figure 7, except for July 21, 2002.

Figure 11 shows the diurnal variation of all variables in local time in order to relate the observed variables to the effects of solar heating occurring as the sun rises and the surface heats. However, on this particular day we can see that the shortwave radiation (Figure 11f) is not symmetric about the time of maximum heating. This asymmetry is introduced due to the presence of clouds. In clear conditions, we would see a smooth bell shaped curve produced by the sun. The long-wave radiation (Figure 11g), shows the emission of the cloud base for low-level clouds in cloudy conditions and the clear sky downward radiation in clear conditions. At night and the early morning, the long-wave radiation is about 400 W m^{-2}. By 11:00, the long wave radiation is decreasing and the short wave radiation is increasing. This is an indicator that the cloud layer is dissipating or burning-off. Along with radiation, there are other indicators such as the temperature and relative humidity that can tell us about surface conditions. We notice that at about 0800 the temperature begins to increase, this continues until max heating is reached at about 1500. The relative humidity (RH), on the other hand, decreases from 90% to about 60% at the time of maximum radiative flux.

C. BOUNDARY LAYER AND CLOUD EVOLUTION

This section will focus on characterizing the evolution of the boundary layer and cloud height using the information obtained from the previous two sections on BLH, cloud depth, and cloudy/clear conditions. Here, we first categorize each measurement day according to the time of cloud break-up on that day. Based on this, we created 9 categories listed in Table 1.

CLOUD AND BOUNDARY LAYER EVOLUTION SUMMER 1999-2003					
CAT	**DEFINITION**	**# OF DAYS(Freq)**	**BLH @ 05:00**	**CLD DEPTH @ 05:00**	**SB (# DAYS)**
1	CLDS Break up before 11	90 (30%)	354	215	13:00 (53)
2	CLDS Break up between 11 and 12	26 (9%)	497	155	14:30 (18)
3	CLDS Break up between 12 and 13	25 (8%)	461	202	14:00 (11)
4	CLDS Break up between 13 and 14	14 (4%)	447	235	14:30 (4)
5	CLDS Break up between 14 and 15	13 (4%)	402	200	13:30 (4)
6	CLDS Persist all Day	85 (28%)	531	237	13:00(29)
7	CLR Between 5 and 15	36 (12%)	1084	N/A	13:30(20)
8	ELSE(Does not meet 1-7)	16 (5%)	545	180	13:00 (6)
9	All Days, All Data	305	456	215	13:30(145)

Table 1. Cloud and boundary layer categories

The number of days meeting category criteria and analyzed for each category are shown in column 3. For each day within a certain category, we obtained the boundary layer height at 0500, about an hour before sunrise. The mean boundary layer height at 0500 for this category is given in Column 4. The mean cloud depth at 0500 for each category is also calculated and listed in Column 5.

Table 1 shows Categories 1 and 6 have the highest frequency of occurrence (30% and 28%, respectively). It appears that about 30% of the summer days (June and July) we have clouds breaking up before 1100 hour and 28% of the time we have full cloud coverage for the entire day. There are 51 days (17%) when clouds break up between 11

and 13 (Categories 2 and 3), while only 8% of the days when cloud break up occurs in the next two hours (Categories 4 and 5). About 12% of the time the MAML is clear of clouds between 0500 and 1500 hour (Category 7).

The BLH before sunrise is compared for each category (Table 1, column 4). It shows that clouds that break up before 1100 is averaged to 354 m, about 150 m lower than Category 2 and about 100 m lower than the other categories with cloud break up (Categories 2,3,4, and 5). However, the cloud depth for this category is about the same as others and no significant difference in cloud depth is seen among the categories, suggesting the cloud base height in Category 1 is much lower than other cloud categories. On the other hand, for those days when clouds persist for the entire day category 6, the boundary layer height before sunrise is the highest among all cloudy cases.

For each category of data, we generated composite diurnal variations of the boundary layer height, the cloud base height, and the cloud depth. This is done by averaging the BLH (or cloud base height) for the same hour from all measurement days within a certain category (column 3, Table 1). Since the cloud base height data from the year 2000 is not available, the number of days used to get the composite cloud base height is usually smaller than the number of days shown in Table 1. An example of the composite BLH and cloud base height for Category 1 is shown in Figure 12.

Category 1 is defined as cases (or days) when cloud break up was seen before 1100. From the total analyzed 305 summer days, 90 days are in this category. Here we do not find significant changes of the cloud top height (or BLH). The cloud base, however, experienced a rapid increase after sunrise (0600 hour) until the cloud breaks up. The cloud depth in this case decreases almost linearly from sunrise to cloud break up (Figure 13). The confidence intervals in both figures indicate that variations in all variables in Figures 12 and 13 are statistically significant.

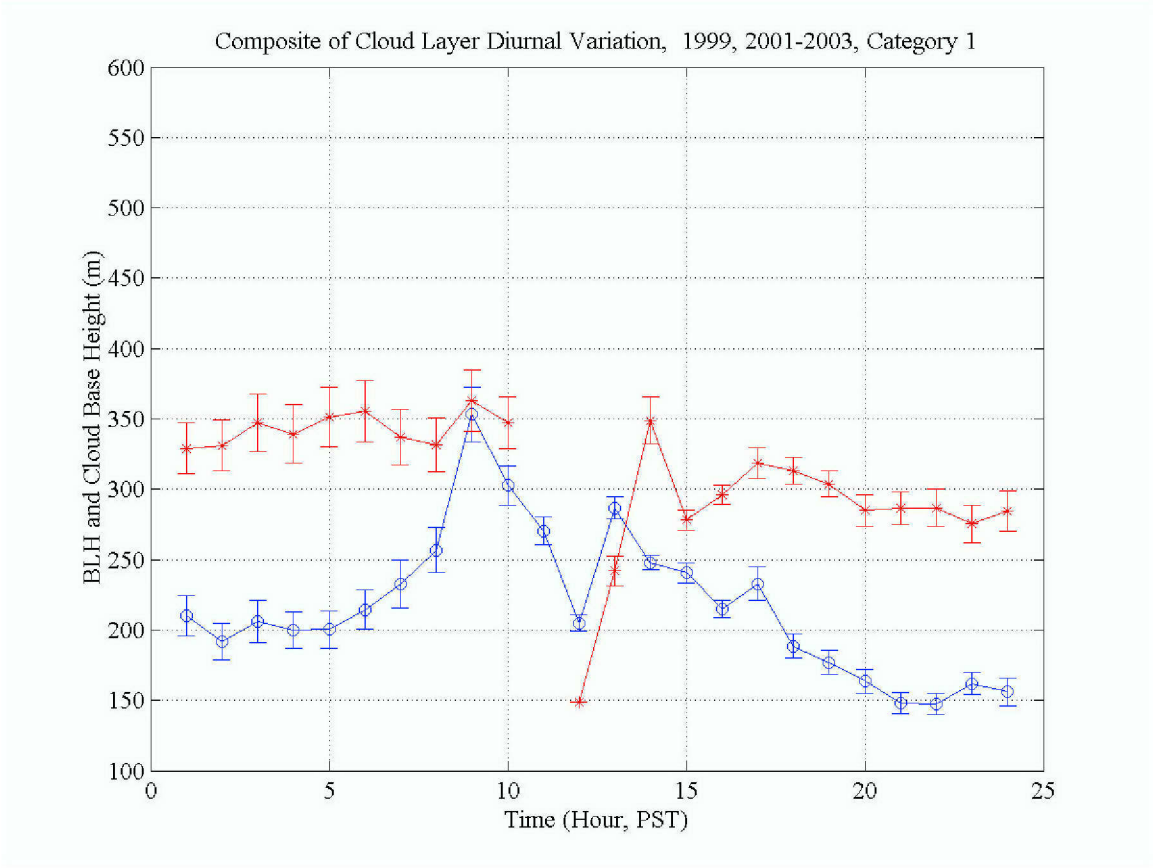

Figure 12. Composite BLH and cloud base height for Category 1 cases. The red line shows the boundary layer top obtained from profiler/RASS profiles; the blue line shows the cloud base height from the CT25K ceilometer. The vertical bars denote the range of the 95% confidence interval.

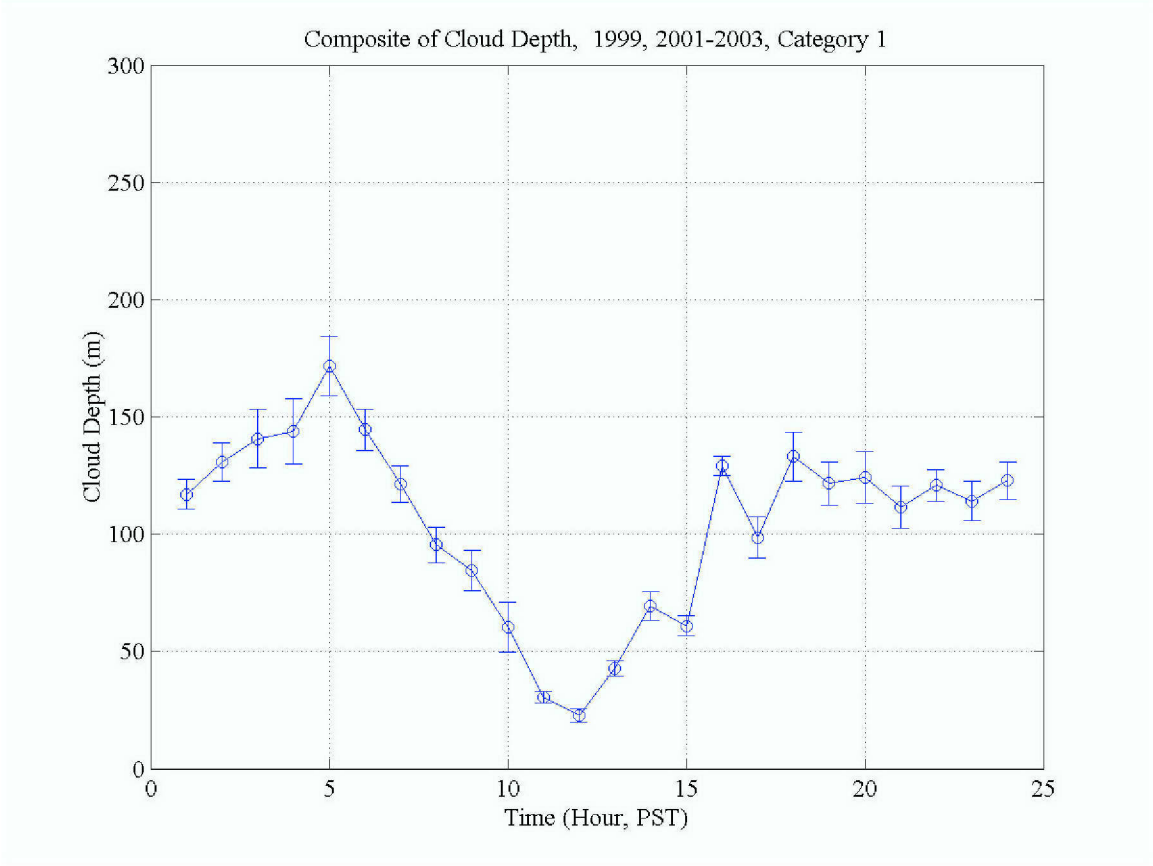

Figure 13. Composite cloud depth variation for Category 1 cases. The vertical bars show the 95% confidence interval.

It is noted that the cloud depth after break up is none-zero in Figure 13. This is caused by the uncertainties in defining cloud/no cloud conditions from different sensors. The cloud/no cloud conditions used to categorize the cases are based on surface radiation measurements as described in Chapter 3. This may not be entirely consistent with the ceilometer-detected cloud. However, Figure 13 indeed indicates less than 50 m cloud depth after 1000 hour, which is qualitatively consistent with our data characterization method.

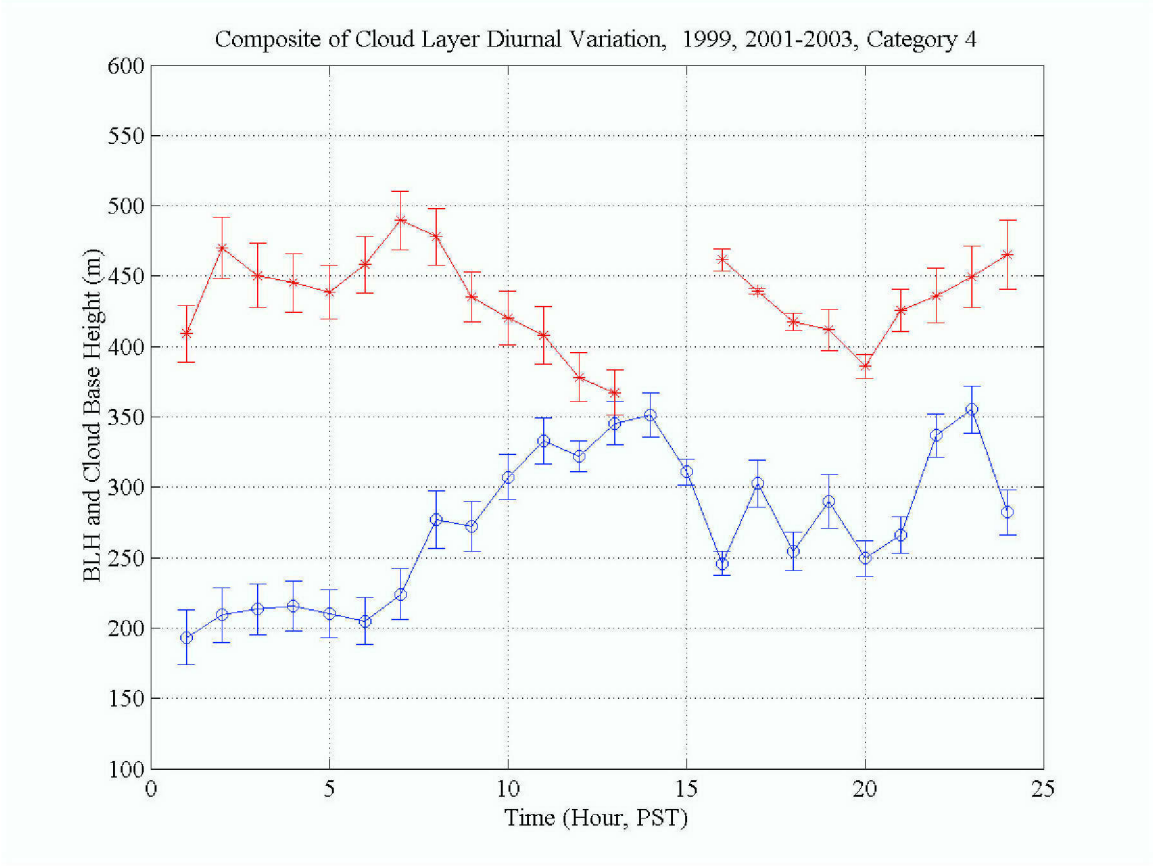

Figure 14. Same as Figure 12, except for Category 4 cases.

Categories 2-5 all show a rather similar pattern of cloud evolution among themselves, but are rather different from Category 1. An example is shown in Figure 14 from Category 4. Here we find an increase of the BLH until 0700 followed by a rapid decrease of the cloud top height. Meanwhile, the cloud base height is stabilized between 200 and 230 m till 0700 hour and quickly increased to its maximum of 350 m by 1400 hour. Figure 15 also depicts this cloud thinning process. We find that the cloud depth increases slightly from 0500 to 0700 and decrease dramatically afterwards until the cloud layer is less than 20 m thick at 1400, which is the cloud break up time. This rapid thinning of the cloud deck is a direct result of the decreasing BLH and the increasing cloud base height.

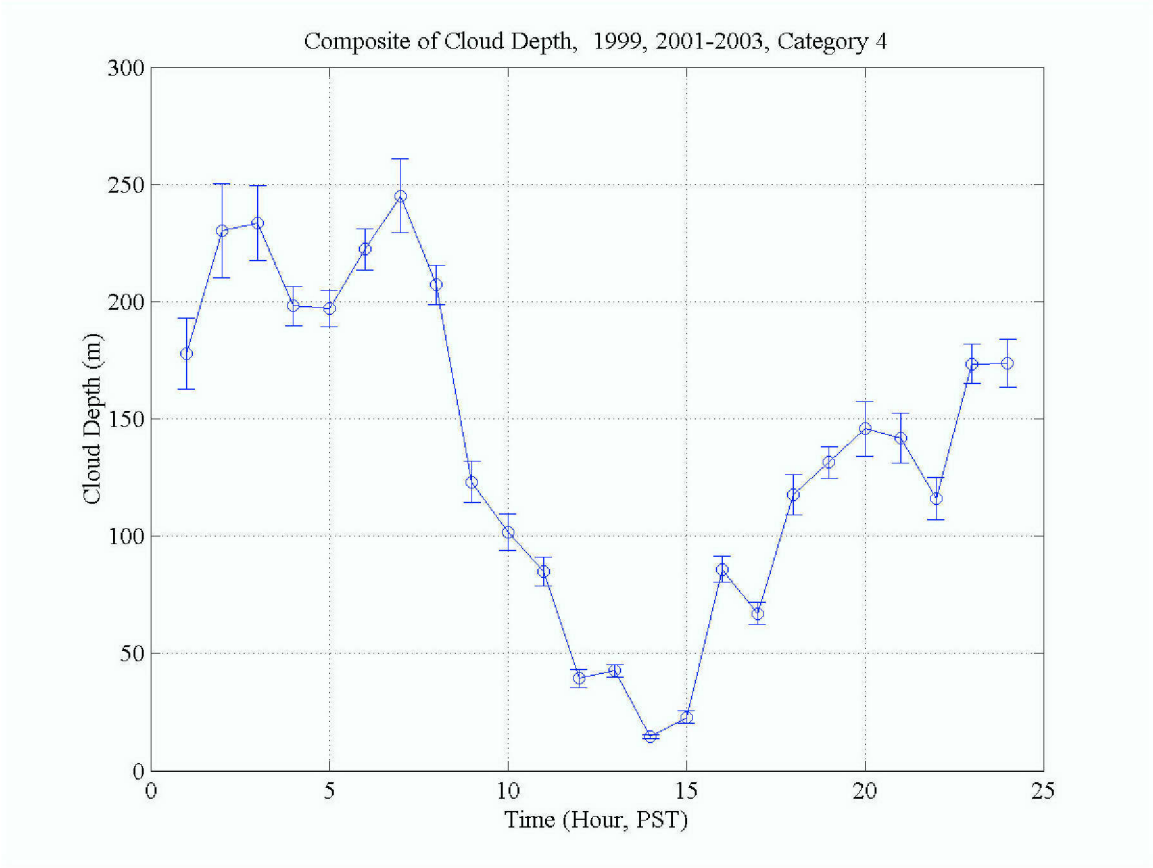

Figure 15. Same as Figure 13, except for Category 4 cases.

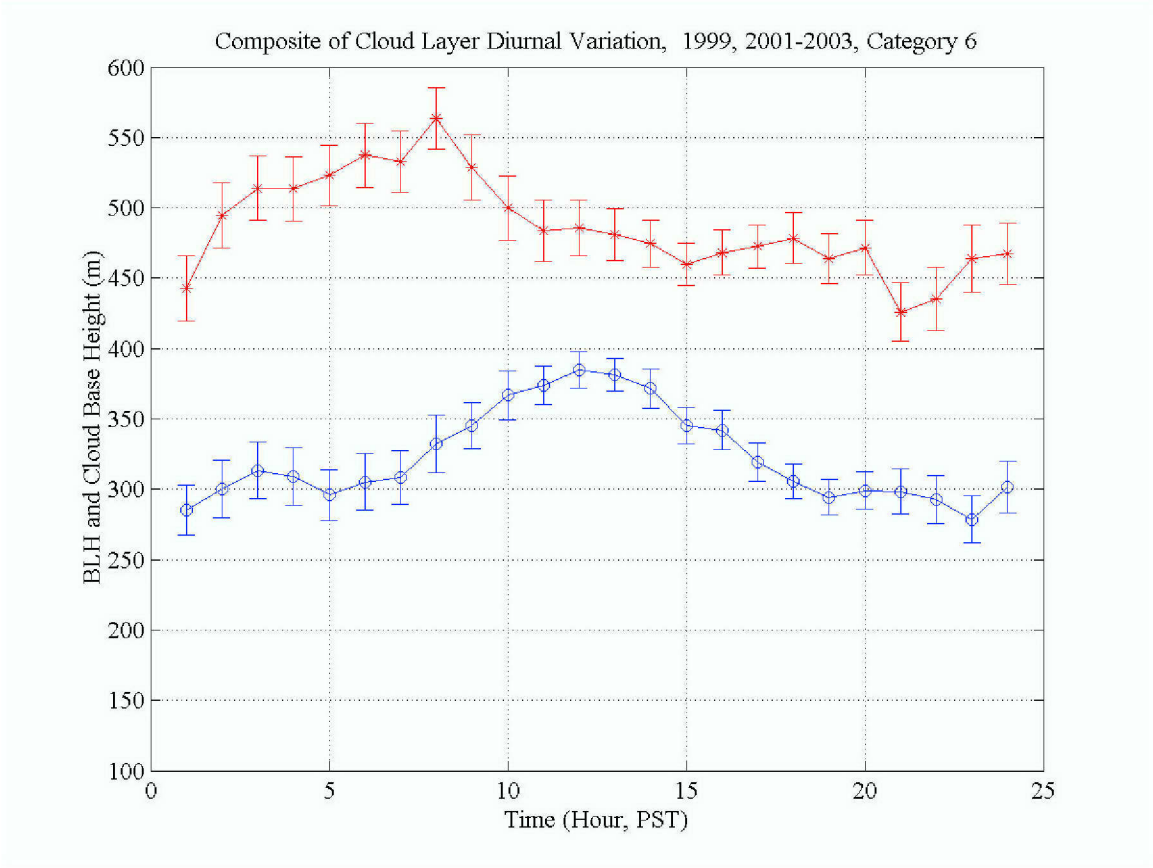

Figure 16. Same as Figure 12, except for Category 6.

Category 6 is for cases when clouds persist all day. This category has the second highest frequency of occurrence, about 28% of the total observations.

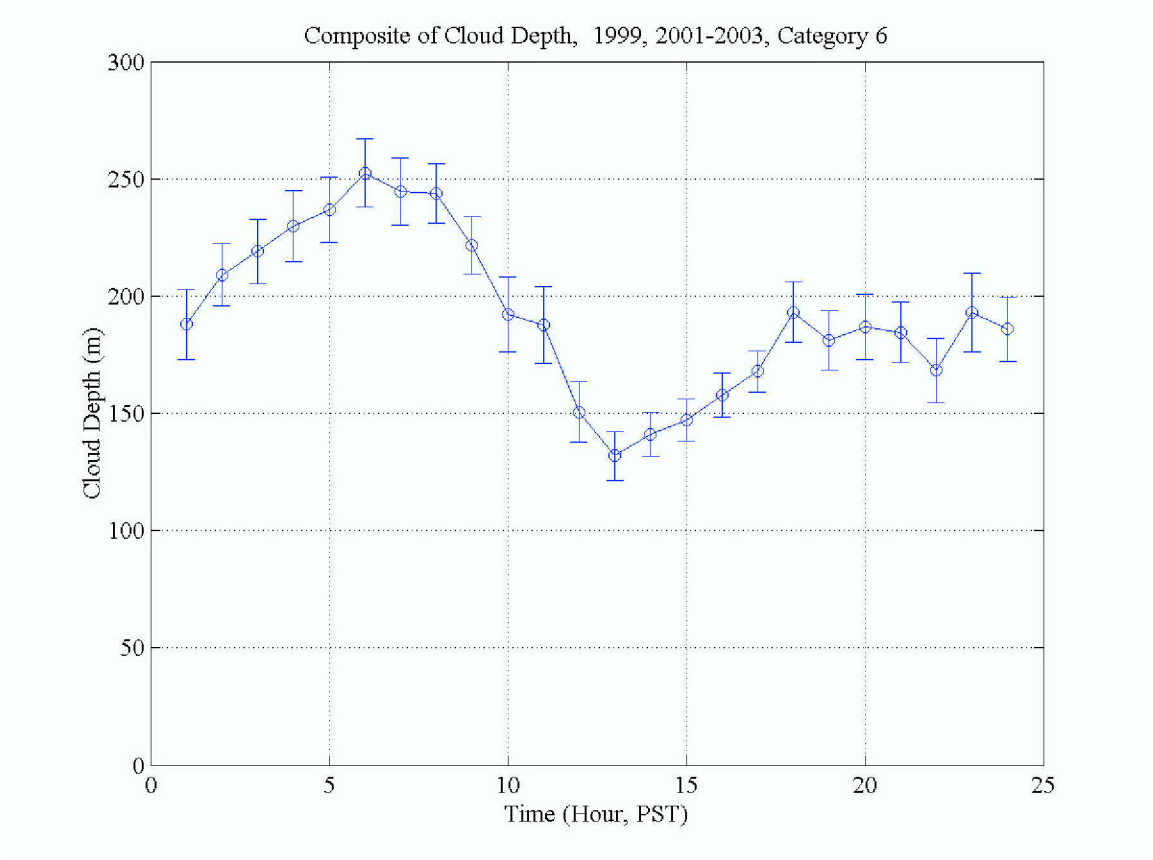

Figure 17. Same as in Figure 15, except for Category 6.

Although the clouds did not break up for this category, the time evolution of the cloud top and of the cloud base is similar to other categories. Increase of the boundary layer height after sunrise is evident and continued until 0800. The decrease of the BLH is also sharp, similar to other categories. The minimum cloud depth reaches 135 m at 1300.

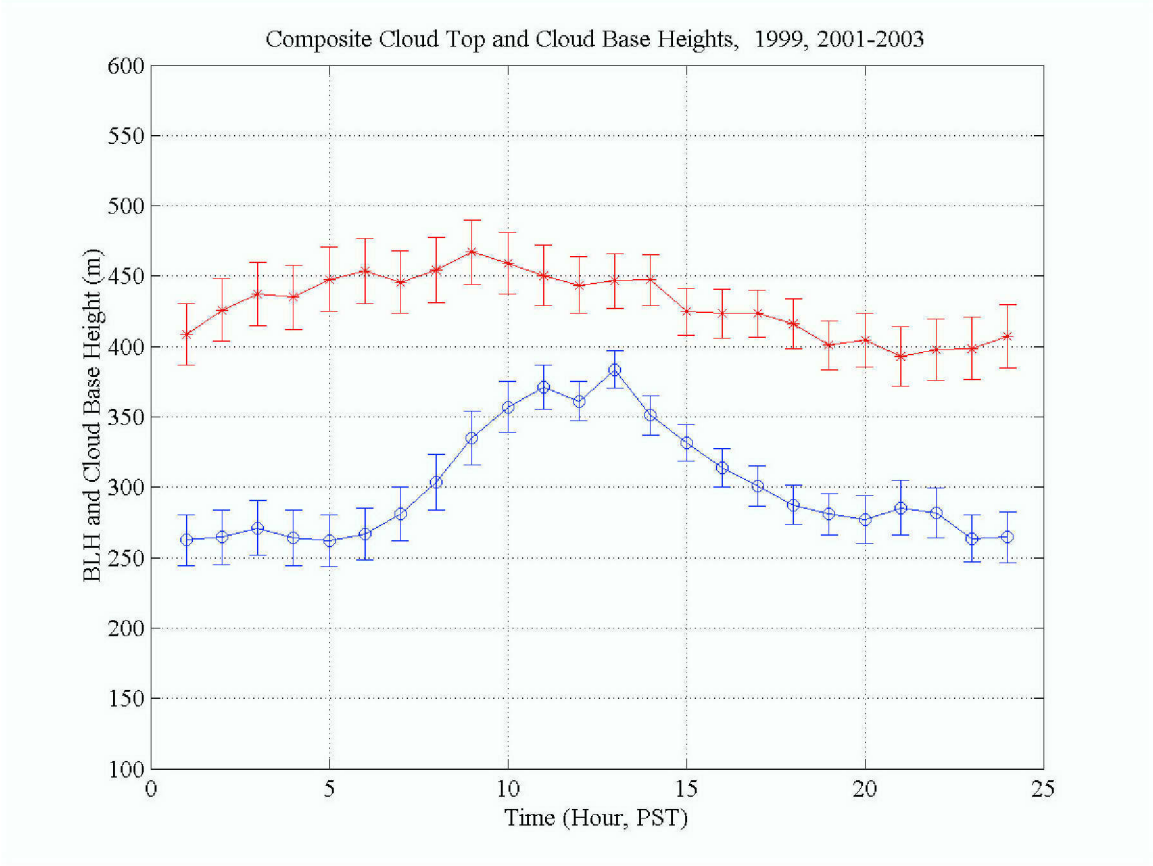

Figure 18. Same as Figure 12, except for all 10-summer months of data used in this study.

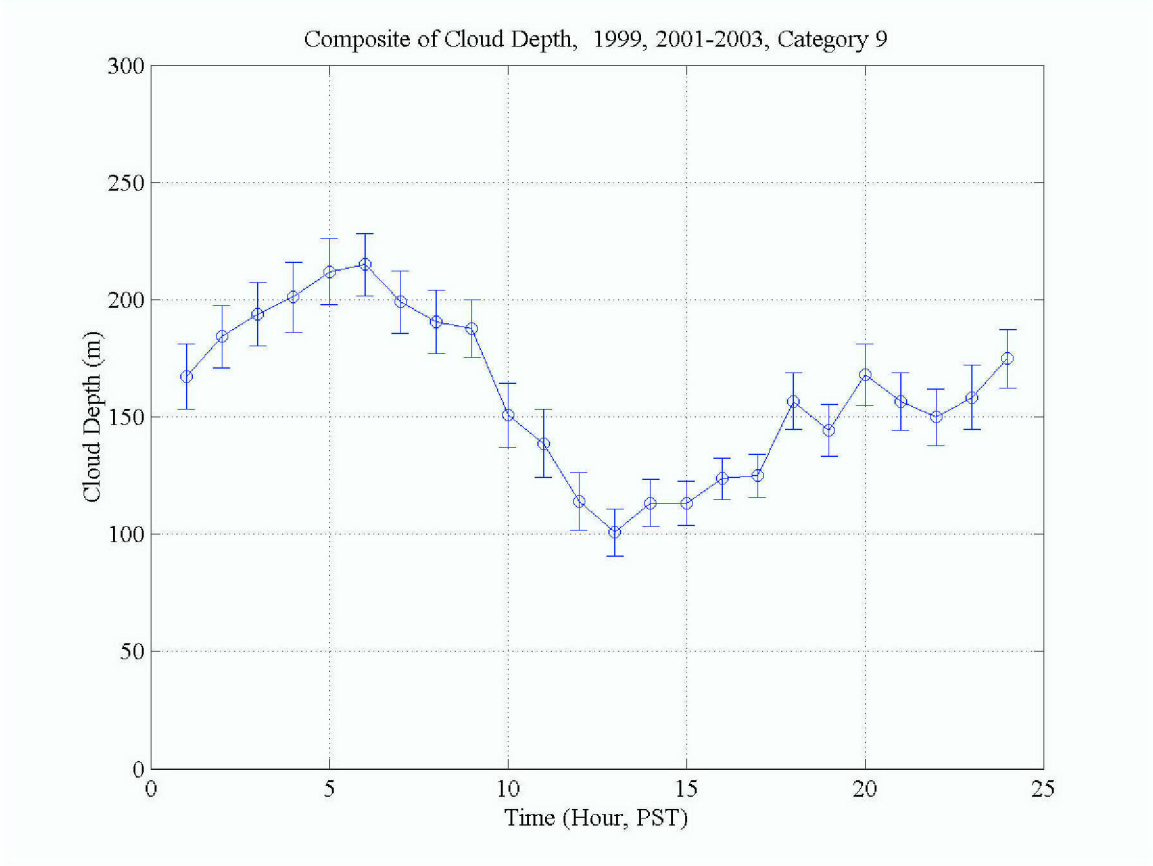

Figure 19. Same as in Figure 15, except for all 10-summer months of data used in this study.

With all the cases involved, the initial increase and the subsequent decrease of BLH, and the increase of cloud base height after sunrise are still evident in Figure 18. The resultant decrease of the cloud depth also shows well in Figure 19 where the thinnest cloud at 100 m is observed to be at 1300 hour. Figures 18 and 19 show the robustness of these results.

To further explore the factors affecting the cloud break up, we can examine the results in Table 1 again. Table 1 shows that the largest mean cloud top height of 531 m at 0500 for this category among all cloudy categories (Categories 1 to 6). The cloud depth appears to be the highest among all cloud categories, but the difference is marginal. From Table 1, we can see the contrast between Categories 1 and 6. Here, the cloud top for Category 6 is about 180 m higher than Category 1. With the cloud depth being about the same, the cloud base height for Category 1 is much lower than that in Category 6.

These findings suggest the role of solar warming in the cloud break up. Since the cloud depth in all categories are similar, the solar radiation reaching the surface below the cloud is likely similar among all cases. After sunrise, when the surface heating and the subsequent turbulent mixing in the boundary layer warms and dries the boundary layer air, the lifting condensation level should increase with time. Since Category 1 has the lowest cloud base height, cloud thinning and early dissipation of the cloud layer is expected.

The enhanced turbulent mixing after sunrise is also consistent with the rise of BLH in the early hours of the morning as enhanced turbulent mixing will result in more entrainment mixing at the cloud top and thus increase the BLH. However, the decrease of BLH after 0900 (Figure 19 and other categories) was unexpected and conflict with the enhanced turbulent mixing. Since entrainment and subsidence are the only two factors affecting the BLH, we infer that there must be enhanced subsidence velocity later in the mornings. In the coastal region, the likely cause of a diurnal variation of the subsidence velocity is sea breeze circulation, which is also associated with the solar heating and land/sea contrast of heat capacity.

D. SEA BREEZE CHARACTERIZATION

The top two plots in Figure 11 are the wind speed and direction, seen in more detail in Figure 20. The wind speed and direction were used to determine the onset and maximum intensity of the local sea breeze. Wind direction just before 1200 is variable and the wind speed is considered light. However, we can see a dramatic change in these conditions at ~ 1200. The wind direction changes from variable to westerly and at the same time the wind speed begins to ramp-up. The wind speed increased from 3 ms^{-1} to about 12 ms^{-1} at 1430. The wind speed increases after sunrise and wind shift times from offshore to onshore were used in this study to collect sea breeze data. The exact time of the shift was used to determine onset and the max wind speed time and intensity were used for duration estimates.

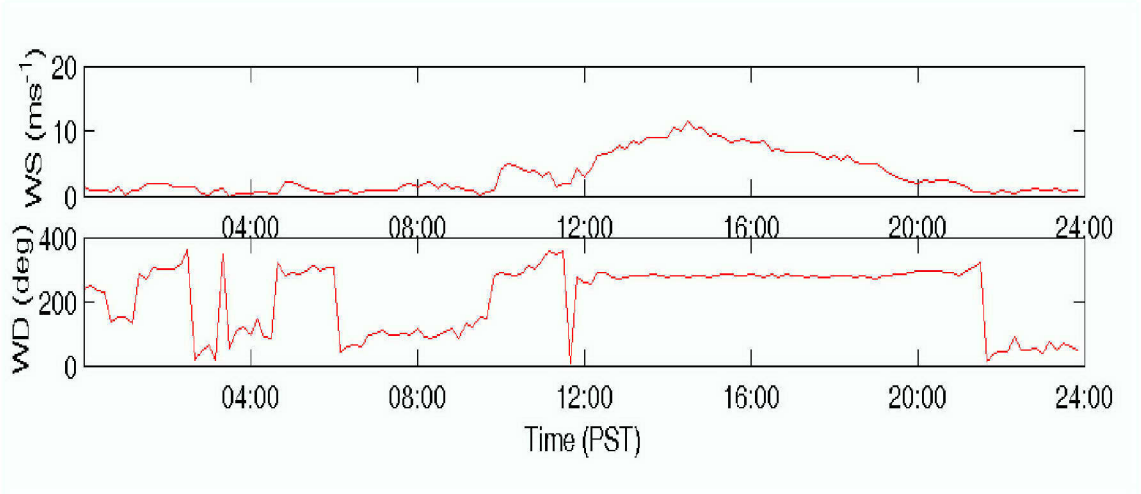

Figure 20. Time variation of wind speed and direction on July 21, 2002. Horizontal axis is time in Pacific Stand Time (PST).

The sea breeze data collected will be used later for statistical analysis. We will try and correlate these conditions to the cloud evolution.

The sea breeze (SB) phenomenon is a result of uneven heating during the daytime between the land and adjacent water. This temperature discontinuity generates a horizontal PGF at the surface from over the ocean toward the land. As a result, air moves toward the land near the surface creating a sea breeze. The scenario presented here is a mesoscale event.

Here, we define the time of wind direction and speed change as the onset of SB. The time when wind speed reaches its maximum and wind direction becomes stable is defined as the time of full development of the SB, which is 1500 for the day shown in Figure 20. The wind variation seen in Figure 20 is typical of those observed at the MAML. In examining the data and categorizing SB onset, we only use the days when the occurrence of SB is apparent. Thus the percentage of SB occurrence here is from a very conservative estimate. Table 2 shows the number days used for the beginning of SB onset, and also the time of SB full development. From the data collected we graphed the observed SB onset time shown in Figure 21 below.

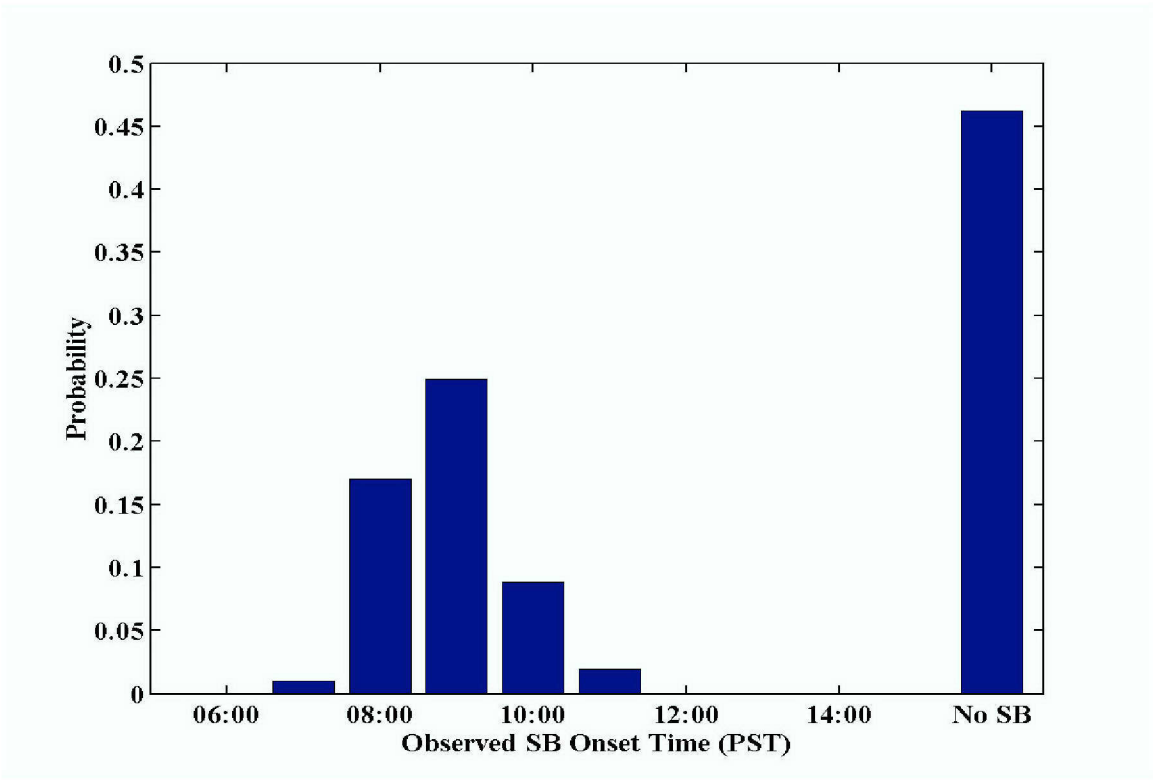

Figure 21. Frequency of occurrence (or probability) of the beginning of SB onset. The non-sea breeze condition (No SB) is listed as a separate category.

Figure 21 shows that 47% of the observations do not have an apparent SB signature in the variation of wind speed and direction. It also shows that most SB onsets occur at 0800 and 0900 with 0900 hour has the largest frequency of occurrence. This is consistent with what has been measured before and reported in the literature since this is the time when the surface begins to increase in temperature.

Once the time of onset was established we then looked at the sea breeze full development time. Full development is determined by looking at the wind speed and measuring the time when the winds reached a maximum velocity and had leveled off. They also maintained that velocity for at least an hour or more. In the example shown in Figure 20, the wind speed associated with full onset was ~12 ms^{-1} and occurred at 1500. The frequency distribution of initial SB onset time is shown in Figure 22 below.

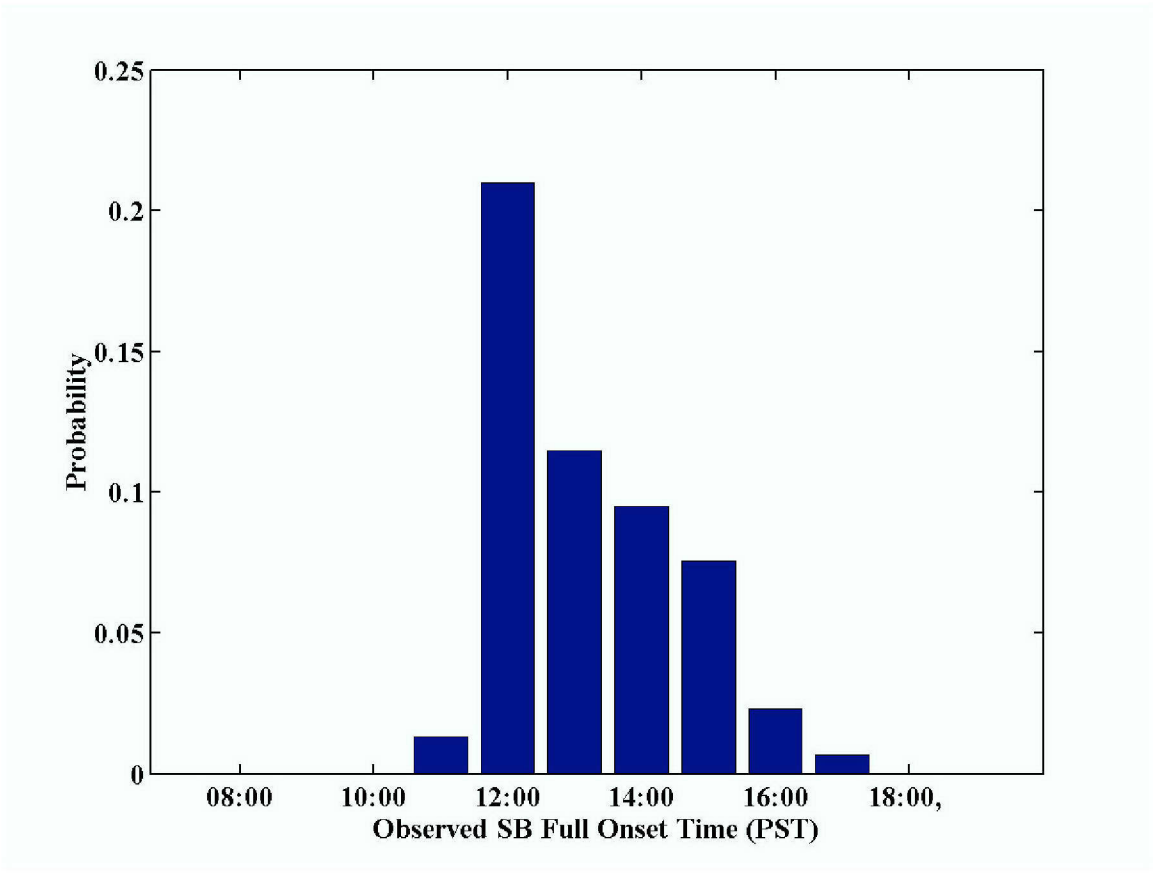

Figure 22. Same as in Figure 21, except for the SB full development time

It shows in Figure 22 that the full onset does not occur until 1100 hour and it peaks at 1200. Full development of the SB is also frequently found between 1300 and 1500. The time of SB full development is also given in Table 1 for each cloud break up category. A comparison of the SB occurrence for the cloud break up categories is interesting. Here, for Categories 1 through 5, the percentage of SB occurrence is 53% (the number of SB occurrence in Column 6 over the total number of days in these categories in column 3). In contrast, only 34% (29/85) of the days in Category 6 shows an apparent SB signature, while about 56% (20/36) of the clear days have a SB. Evidently, the occurrence of the SB is preferred in clear or partially clear days and it is least likely in the days will full cloud coverage. Does the presence of clouds prevent the formation of a SB circulation, or does a SB occurrence result in the breakup of clouds? The full interaction between the SB and the coastal clouds is yet to be understood, but is beyond the scope of this thesis research. Nevertheless, the frequent occurrence of SB during the measurement days suggests that the decrease of boundary layer height seen in

previous section can be associated with the presence of SB. In addition, the SB front probably lies further inland from the MAML site so that the SB enhances the local subsidence at MAML. In the next Chapter, we will examine how the enhanced subsidence may affect the timing of cloud break up using a simple mixed layer model.

This model will allow us to simulate the evolution of the cloud layer and the boundary layer from sunrise to the time of cloud break-up. This simulation will aid in the understanding of the relationship between the SB and the BLH and their diurnal evolution.

THIS PAGE INTENTIONALLY LEFT BLANK

V. MODEL SIMULATION AND DISCUSSION

A. SIMULATION OBJECTIVES AND 1D MODEL OVERVIEW

From the previous chapter, we have examined the evolution of the BLH, cloud base height, and the cloud depth and identified their association with time after sunrise and the SB circulation. The effects of surface heating and enhanced subsidence due to the SB circulation will be examined carefully in this chapter to illustrate how these two processes contribute to the timing of cloud break up. A 1-dimensional cloud mixed layer model will be used for this purpose.

One-dimensional cloud mixed layer models have been used frequently in the past to study the physical processes occurring in the stratocumulus-topped boundary layers (e.g., Lilly 1968, Nicholls 1984). Because of its simplicity and direct link to the physical processes, this type of model is ideal for testing hypotheses or cloud parameterizations. In this study, we modify the mixed layer model over the ocean surface to use over land surfaces so that we can use it to study the effects of increased surface fluxes on cloud break up.

B. MOIST MIXED LAYER MODEL:

The prognostic variables in the moist mixed layer model are equivalent potential temperature (θ_e), total water specific humidity (q_T), and boundary layer height (or equivalently, cloud-top height, h). Depending on the treatment of radiation, the prognostic equations are different, as discussed below.

1. Non-Interactive Radiation

For simplicity, we consider the cloud layer as a dust layer, or dry cloud layer which means that the cloud-top radiation is not affected by cloud microphysics. Hence the cloud radiative property can be represented by a constant F_{rad} that is the difference between the total radiative flux at the inversion base and that at the boundary layer top. To further simplify the problem, we assume that the radiative cooling occurs entirely in the inversion layer. In other words, radiative cooling affects the boundary layer

turbulence through the cooling of the inversion air and therefore causes entrainment directly. In this situation, the prognostic equations are:

$$\frac{\partial \theta_e}{\partial t} = \frac{(\overline{w'\theta'_e})_0 - (\overline{w'\theta'_e})_h}{h}$$
$$\frac{\partial q_T}{\partial t} = \frac{(\overline{w'q'_T})_0 - (\overline{w'q'_T})_h}{h}$$
$$\frac{\partial h}{\partial t} = \frac{-(\overline{w'\theta_v})_h + F_{rad}}{\Delta\theta_v} - DIV \cdot h$$

where F_{rad} is a constant given in the input file. For the layer of stratocumulus clouds, reasonable values of F_{rad} range from 40 to 100 ms^{-1} K.

2. Interactive Radiation

The cloud radiative properties are closely related to the thermodynamics and microphysics of the cloud layer. Therefore, realistic boundary layer cloud simulations should allow the cloud radiative field to vary with the cloud properties. This is the interactive radiation. For simplicity, we assume that radiative cooling occurs only in the cloud layer, which is inside the boundary layer. In this situation, the prognostic equations for θ_e, q_T, and h are:

$$\frac{\partial \theta_e}{\partial t} = -\frac{\partial(\overline{w'\theta'_e})}{\partial z} - \frac{\partial R}{\partial z}$$
$$\frac{\partial q_T}{\partial t} = -\frac{\partial(\overline{w'q'_T})}{\partial z}$$
$$\frac{\partial h}{\partial t} = -\frac{(\overline{w'\theta_v})_h}{\Delta\theta_v} - DIV \cdot h$$

Here, the radiative flux profile (R) is calculated internally at the user specified time and vertical space intervals. The radiation scheme uses the emissivity approach described in Rodgers (1976). Also note that solar radiation is not included in the radiation scheme. As a result, we consider the model designed for a nocturnal marine cloudy boundary layer.

The parameterization for cloud-top entrainment follows that of Nicholls *et al* (1986). Basically, entrainment is related to two parameters, one is the interfacial

Richardson number (R_i), the other is the integrated buoyancy deficit (Δ_m) caused by evaporation of cloud water through entrainment:

$$\frac{w_e}{w_*} = \frac{C_1}{R_i}[1 + C_2(1 - \frac{\Delta_m}{\Delta\theta_v})]$$

where Ri is defined as $\frac{gh\Delta\theta_v}{\theta_v w_*^2}$. This quantity is related to the stability of the inversion air. C_1 and C_2 are constants, determined from observational data. For stratocumulus clouds in the mid-latitudes, C_1 is usually 0.2, and C_2 is 60. Δ_m is defined by $2\int_0^1 \delta\theta_v \, d\varepsilon$, where ε is the entrainment mixing fraction, $\delta\theta_v$ is the difference in virtual potential temperature between the mixed parcel and that of the boundary layer. It is a function of ε, temperature and moisture in both the inversion air and the boundary layer. You can change the value of C_1 in the model input file. This allows you to see the sensitivity of your cloud and boundary layer to entrainment effects.

The following diagnostic equations describe the relationships among some of the variables used in the model. These equations help to analyze the model output.

Below cloud:

$$\overline{w'\theta'} = \overline{w'\theta'_e} - \frac{L_v}{C_p}(\overline{w'q'_T})$$
$$\overline{w'\theta'_v} = \overline{w'\theta'_e} - (\frac{L_v}{C_p} - \psi\theta)(\overline{w'q'_T})$$
$$\overline{w'q'} = \overline{w'q'_T}$$

In cloud:

$$\overline{w'\theta'} = \overline{w'\theta'_e} - \frac{L_v}{C_p}(\overline{w'q'_T} - \overline{w'q'_l})$$
$$\overline{w'\theta'_v} = \beta\overline{w'\theta'_e} - \theta(\overline{w'q'_T})$$
$$\overline{w'q'} = \frac{dq_{sat}}{d\theta}\overline{w'\theta'}$$

where

$$\beta = \frac{1 + (1+\psi)\theta \frac{dq_{sat}}{d\theta}}{1 + \frac{L_v}{C_p}\frac{dq_{sat}}{d\theta}}$$

ψ=0.608, L_v and C_p are the latent heat of vaporization and specific heat under constant pressure, respectively ($L_v = 2.5 \times 10^6$ Jkg^{-1}, $C_p = 1005$ J kg^{-1}K^{-1}). Note that β varies slowly with temperature and is typically ~ 0.6. We assume that cloud layer in the model is always saturated so that the water vapor specific humidity is a function of temperature by Clausius-Clapeyron.

Wang et al (1999) adapted the above described model over coastal land by replacing the bulk parameterization for surface sensible and latent heat flux with a specified time variation. In their simulations, the surface sensible heat flux was given as a sinosoidal function:

$$F_{hs} = F_{s0} + F_{hsa} \sin(t - 6) \qquad \text{Eq. (A)}$$

where $F_{hs0} = 1$ Wm^{-2} was set as the minimum sensible heat flux at sunrise (0600) and $F_{hsa} = 100$ Wm^{-2} is the amplitude to specify maximum sensible heat flux after sunrise. By 1200, the sensible heat flux would reach its maximum of 101 Wm^{-2}. The moisture flux is set at a constant of 25 Wm^{-2}. The same setting will be used in this study. Since strong variations are found in the surface heat flux over different land surfaces with a variety of moisture capacities, these values are taken arbitrarily, but are within the range of the frequently observed values over semi-arid surfaces. However, the model is mainly used to illustrate the effects of the surface fluxes, not as a tool to predict the time of cloud break up. Therefore, different choices of the surface flux values should not affect the conclusions from this model study.

C. MODEL SETUP AND SIMULATION RESULTS

The initial condition used in the model is the same as those from Wang et al (1999). The model simulation was made for July 6, 1999 where rawinsonde measurements were made at multiple times at night and after sunrise (Wang et al., 1999).

The simulation started at 0600 (PST) and continued until cloud break-up. Figure 23 shows the model initial vertical profile of files of potential temperature (0600 PST, or 1300Z), modeled temperature profile at 1 hr into the simulation together with the observed profiles at the same time.

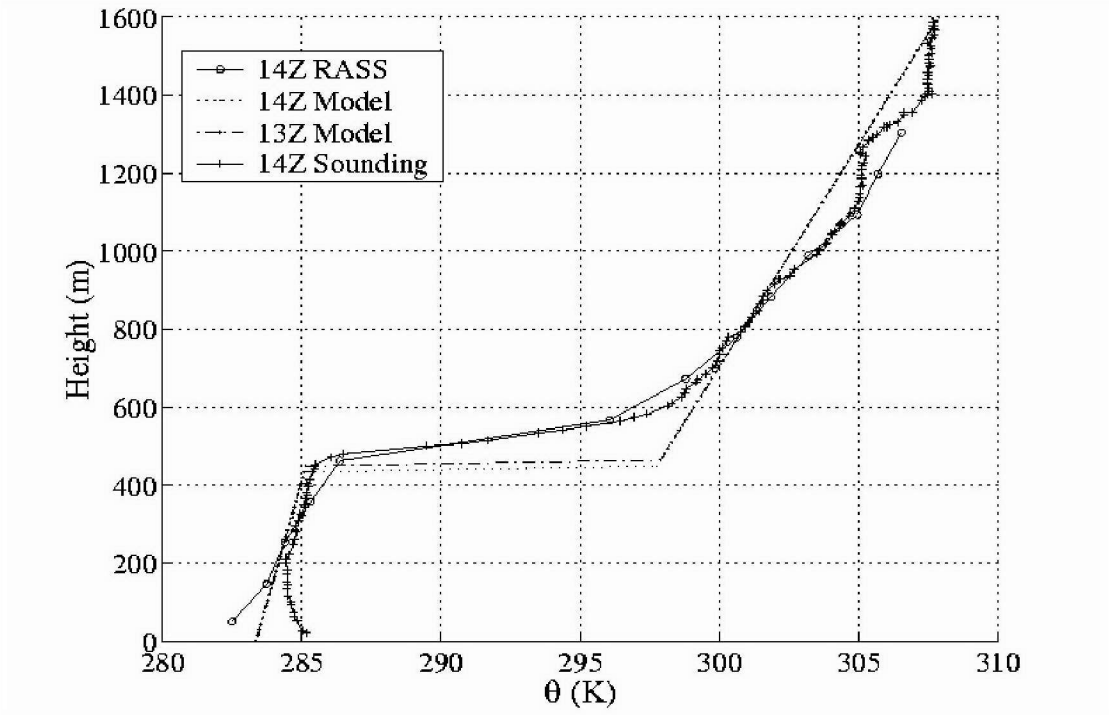

Figure 23. Comparison of model initial conditions

MOIST MIXED LAYER MODEL				
CASES	**SURFACE FLUX**	**DIVERGENCE**	**BREAK-UP TIME**	**BLH AT BREAK-UP**
CNTRL	FIXED(25 Wm^{-2})	FIXED ($2.0x10^{-6}s^{-1}$)	NONE	N/A
SFCflx	Eq. A	FIXED ($2.0x10^{-6}s^{-1}$)	1340	580 m
SBwk	Eq. A	Eq. B	1230	495 m
SBstrg	Eq. A	Eq. B	1200	450 m

Table 2. Case settings of the 1-d model simulation

Table 2 shows a listing of the four simulations (cases) to be done in this study. The series of simulations are designed to test the effects of surface fluxes and enhanced subsidence on the evolution of the boundary layer and cloud properties. The control case

(CNTRL) uses a fixed low sensible heat flux of 25 W m^{-2} with no change in subsidence driven divergence. An increase of the surface heat flux is introduced in case SFCflx where the sinusoidal heat flux increase for the first quarter of a period is used (Eq. A). These two simulations were done in the study of Wang et al. (1999), but are repeated here in order to show the difference enhanced subsidence makes. In case SBwk, a weak linear increase of subsidence driven divergence is introduced into the simulation to mimic the onset of the SB and its development two hours after sunrise. In case SBstrg, we used a stronger SB divergence to illustrate the sensitivity to the cloud evolution of the subsidence. The time variation of the divergence is given in Eq. (B) below.

$$\begin{aligned} &\text{divgrd} = 2\text{x}10^{-10}\ \text{s}^{-2}\ (\text{t} < 7200\text{s}) \\ &\text{divgrd} = 5\text{x}10^{-10}\ \text{s}^{-2}\ (\text{t} < 7200\text{s})\ \ (\text{SBwk}) \\ &\text{divgrd} = 1\text{x}10^{-9}\ \text{s}^{-2}\ (\text{t} < 7200\text{s})\ \ (\text{SBstrg}) \end{aligned} \qquad \text{Eq. (B)}$$

The surface heat flux variations for all cases are shown in Figure 24 and the subsidence driven divergence is given in Figure 25. For all cases, both the surface flux and the divergence forcing are plotted until the time of the simulated cloud break up.

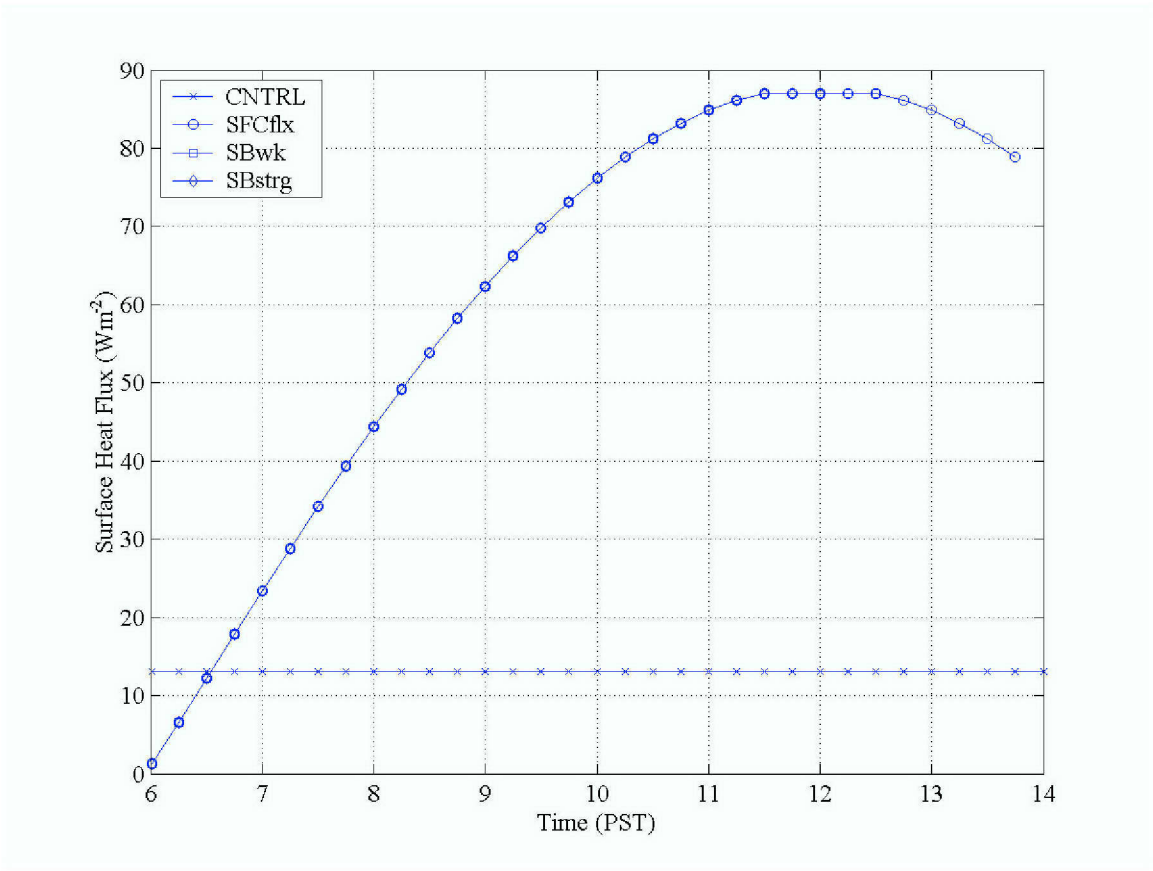

Figure 24. Surface heat flux input used in all four simulated cases.

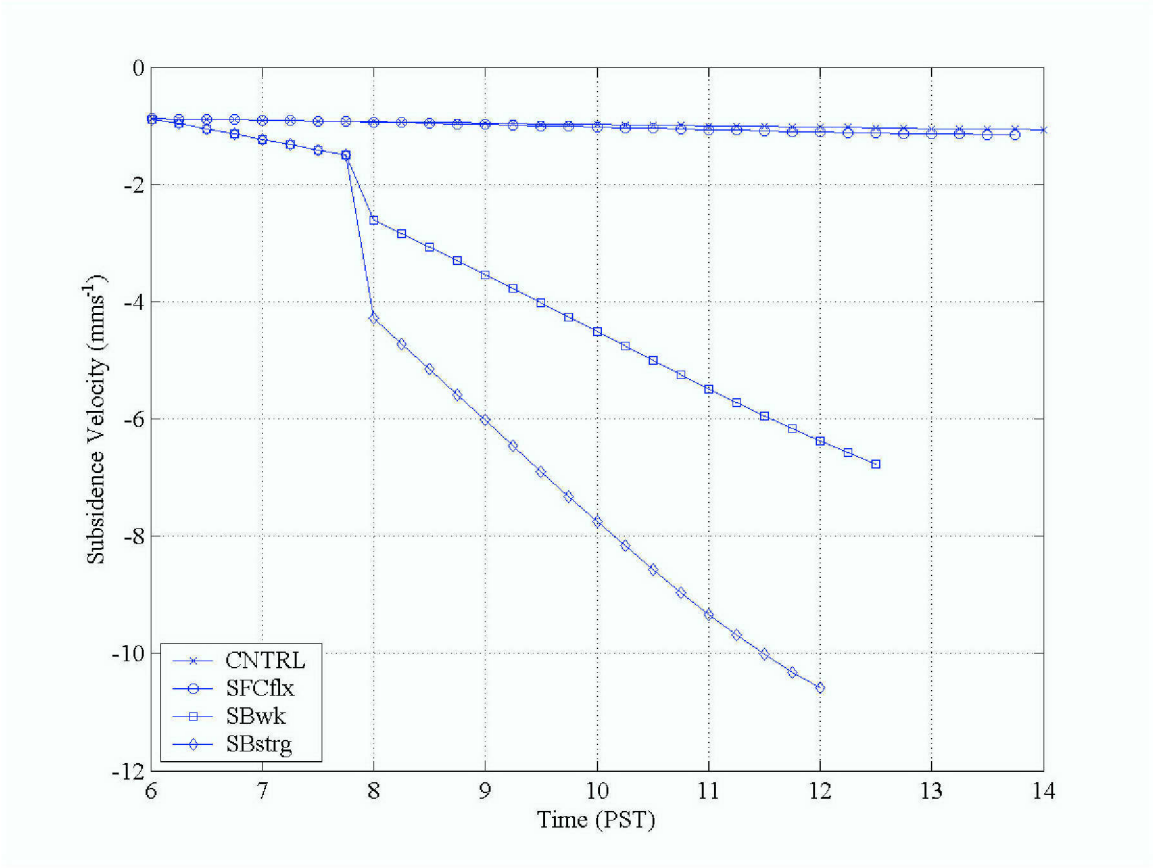

Figure 25. Subsidence velocity for all four simulated cases.

Figure 26 shows a comparison of the BLH and cloud base height evolution for all four cases. Here, the CNTRL case shows the lowest cloud base height and no sign of cloud break up. With the increase of surface flux in case SFCflx, BLH height increases rapidly, and the cloud base height increases even more rapidly, resulting in rapid thinning of the cloud layer and the cloud break up at 1340. The boundary layer height at this time is at 580 m.

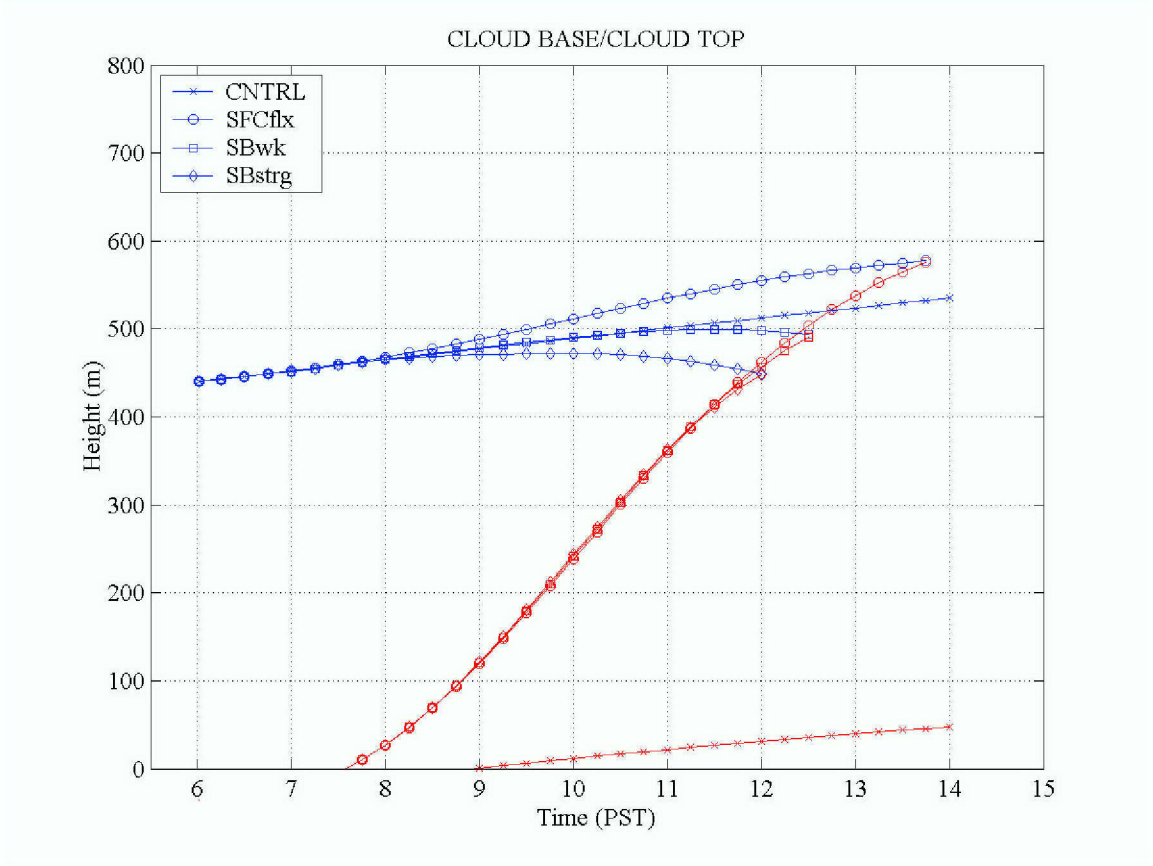

Figure 26. Evolution of cloud base and cloud top height for all four simulated cases.

In case SBwk, the increase in SB subsidence results in cloud break-up at 1230, almost an hour earlier than in the SFCflx case. Here, the BLH increases initially and begins to transition to a lower level right before the cloud break up at a BLH of 495 m. This is a difference of ~100 m from the SFCflx case. The results here indicate that through the use of increased divergence we are able to produce a similar reaction to the atmosphere that could be seen in our observed data sets. In order to make the correlation between a divergence increase and the BLH decrease we ran one more case in which we further increased the divergence. This can be seen in the forth case.

In the SBstrg case, even greater divergence is used after 0800. This adjustment resulted in an even earlier cloud break-up at 1200, about a half hour earlier than in the SBwk case and an hour and a half before break-up in the SFCflx case. Again we see the cloud top or the BLH begin to decrease just prior to cloud break-up. The boundary layer in this case lowers to about 450 m showing a difference of about 50 m from the SBwk

case. This case clearly showed that increased divergence does play a major roll in lowering of the BLH just prior to cloud break-up.

Figure 27 shows the convective velocity, w_*, in the four cases.

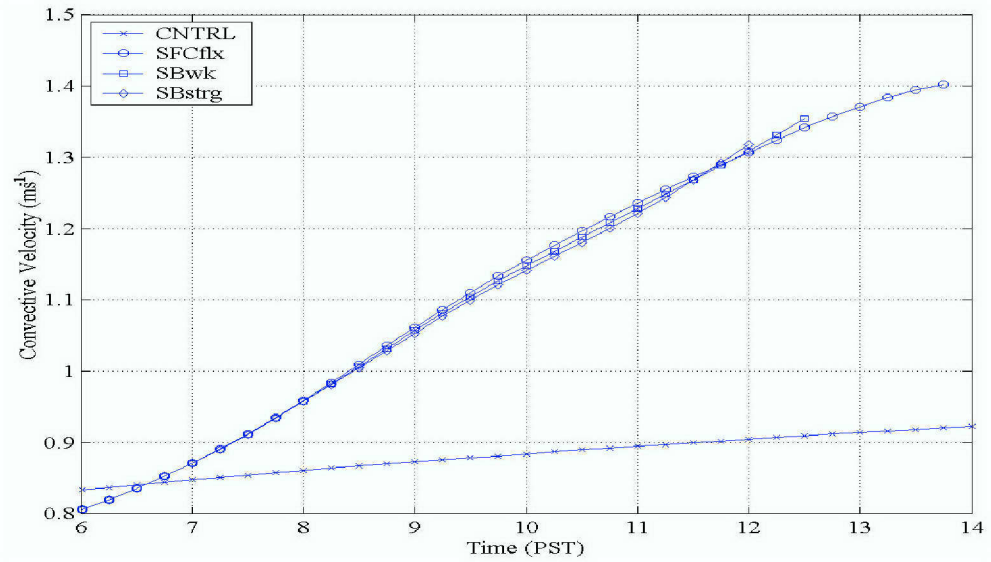

Figure 27. Convective velocity from all simulated cases.

The convective velocity represents the level of turbulence in the convective boundary layer. Figure 27 shows the increase of w_* in all cases where the surface flux is enhanced, suggesting the role of surface heat flux in enhancing turbulent mixing in the cloud mixed layer. The increased turbulence kinetic energy hence leads to a significant increase of the entrainment velocity (Figure 28) in all three cases.

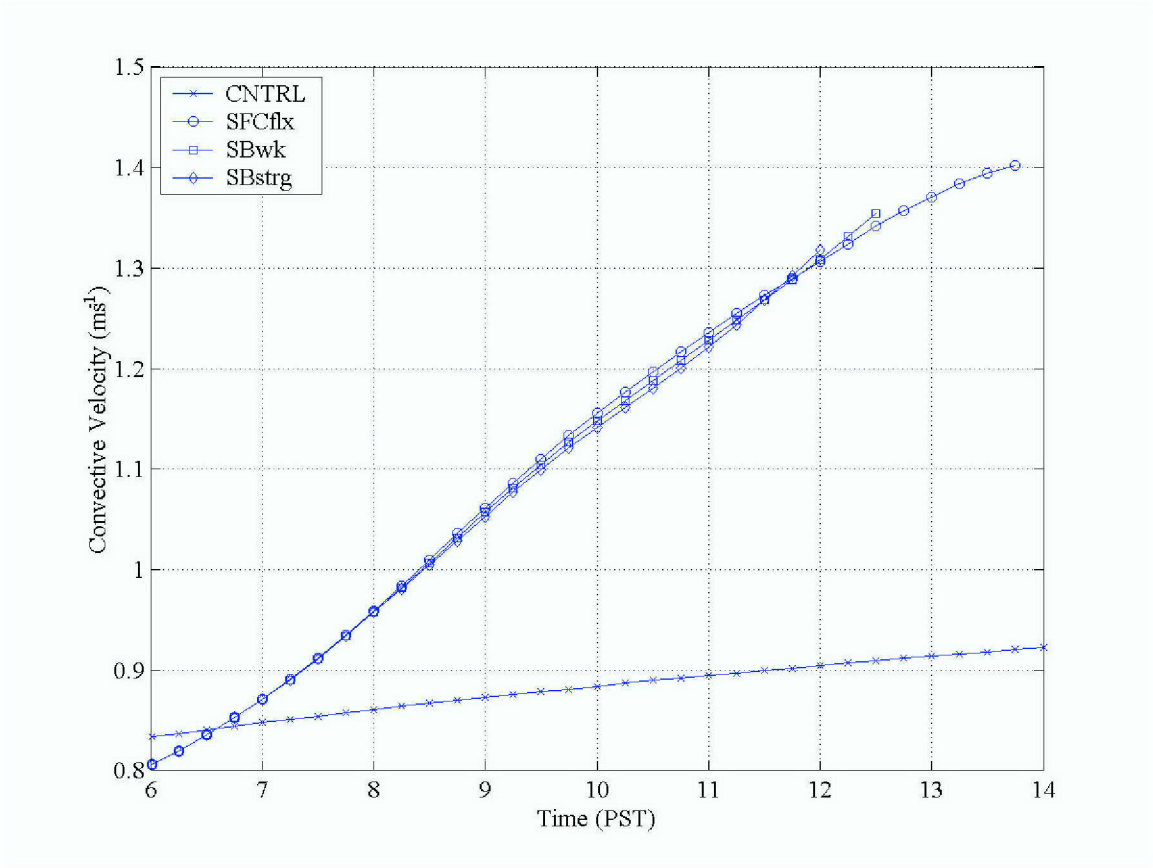

Figure 28. Entrainment Velocity for all simulated cases

Next we will discuss the effect of surface heat flux on the evolution on boundary layer temperature, water vapor, and cloud water. Since the three test cases (SFCflx, SBwk, and SBstrg) are similar, we will mainly look into the differences between the control case (CNTRL) and the surface flux case (SFCflx).

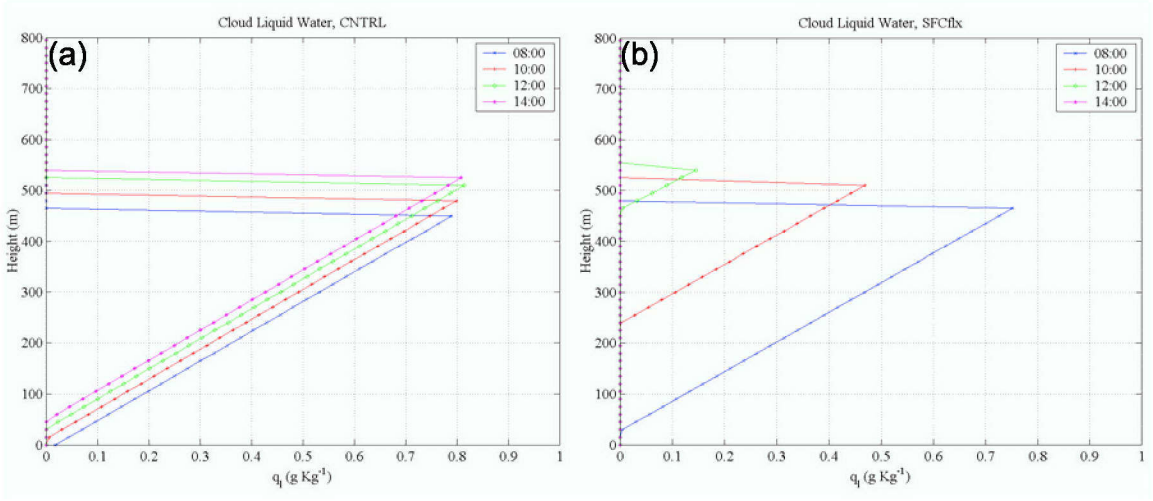

Figure 29. Cloud Liquid Water evolution in control case (a) and in case SFCflx (b).

Figure 29 shows the cloud layer evolution using the cloud liquid water content (q_l). Figure 29 has a CNTRL case on the left and a SFCflx case on the right. Liquid water in the clouds increases with height in both cases, which is the product of the adiabatic liquid water assumption for the mixed layer model. For the control case, both BLH and cloud base height increase slowly and the maximum liquid water content stays about the same since the cloud layer depth is nearly unchanged. In the SFCflx case, however, cloud base increases rapidly as seen in Figure 29b. The decrease in cloud depth results in greatly reduced cloud liquid water. By 1400 the clouds have broken-up.

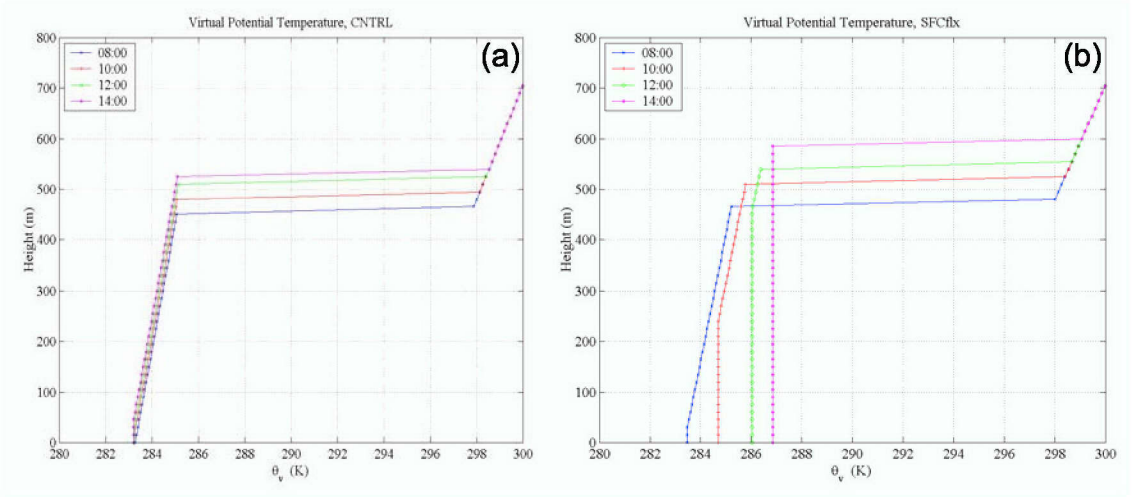

Figure 30. Virtual Potential Temperature evolution in control case (a) and in case SFCflx (b).

Figure 30 shows the boundary layer temperature evolution. The CNTL case is on the left and the SFCflx case is on the right. The SFCflx case shows an increase in (θ_v) from 283.5 K at 0800 to 287 K at 1400. The boundary layer height also increases from 475 m to 590 m respectively. The BLH grows until cloud break-up.

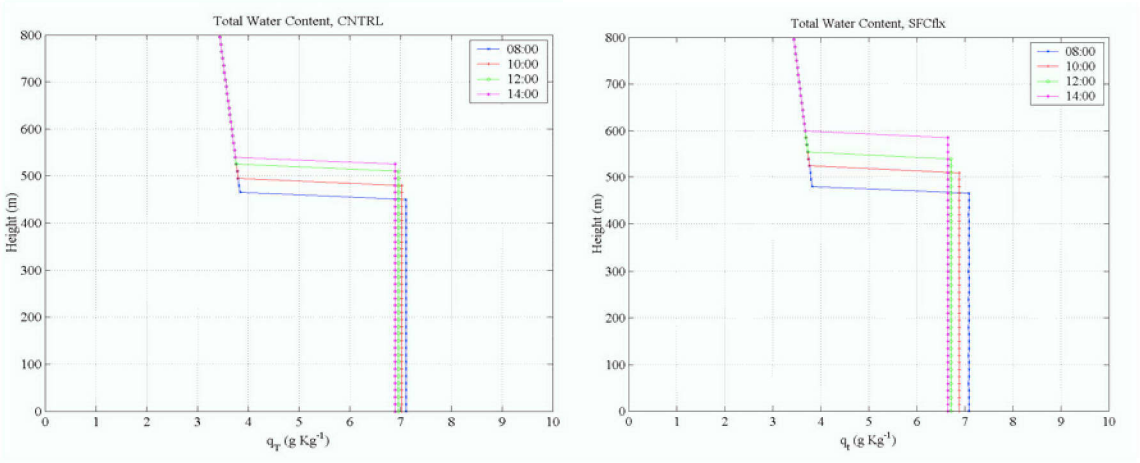

Figure 31. Total water content and its time evolution in control case (a) and in case SFCflx (b).

Figure 31 shows the boundary layer total water evolution. We can see that the boundary layer dries at a faster pace for case SFCflx compared to the control run. While the warming is the combined effects of surface heating and entrainment, the drying of the boundary layer is dominated by the increase of entrainment velocity in case SFCflx (Figure 31b). Figures 30 and 31 suggest a warming and drying of the boundary layer, both contribute to a higher lifting condensation level (LCL). The higher temperature and the drier boundary layer lead to a higher LCL and eventually dissipate all the cloud water by having an LCL at the top of the boundary layer.

The simulated cases here show the dominant effect of surface heat flux in promoting stronger turbulent mixing and hence stronger entrainment at the boundary layer. As the result, the boundary layer becomes increasingly warmer and drier and eventually leads to the total dissipation of the cloud layer. On the other hand, the sea breeze circulation modulates the cloud break up process and leads to an early break up of the cloud layer with a lower cloud top. The timing of the cloud break up is dependent on the magnitude of the subsidence velocity.

THIS PAGE INTENTIONALLY LEFT BLANK

VI. CONCLUSIONS AND RECOMMENDATIONS

A. SUMMARY AND CONCLUSIONS

The objective of this thesis is to understand the evolution, composition and diurnal transition of the marine boundary layer along the coast of California. Using the NPS wind profiler/RASS system, vertical profiles of virtual potential temperature were generated hourly for June and July from 1999 to 2003. These summer months were chosen because of the frequent occurrence of coastal stratocumulus clouds and the subsequent cloud break up over the coastal land.

Boundary layer height was obtained from each hourly profiler/RASS profile for the entire dataset. For each hour, we also obtained the cloud/no cloud condition using a combination of solar and infrared radiation measurements. Using the wind direction and speed measurements from the NPS MAML met station, we also obtained the time of sea breeze onset and the time when the sea breeze is fully developed. In addition, cloud base height from a laser ceilometer was also examined and saved on the time stamp of the boundary layer height. These data products were then analyzed to reveal the characteristics of the boundary layer and cloud evolution and their relation with the sea breeze circulation.

In order to characterize the cloud breakup and the processes affecting the cloud break up, all the products were grouped into different cloud categories and statistics were made for each category. Diurnal variation of the boundary layer height, cloud base height, and the cloud depth were then examined.

The diurnal evolution of the boundary layer showed the growth of the layer from sunrise. However, lowering of the BLH was found to dominant all cloud break-up categories. Also, the cloud base height increased rapidly after sunrise until the clouds broke-up. It was evident in the analysis that the cloud layer thinned and eventually dissipated. In terms of the timing of the cloud break up, the results showed earlier break up for lower cloud decks since the cloud depths for all categories were about the same.

The unique evolution of this break-up was evidently associated with solar radiation. However, lowering of the BLH cannot be caused by solar heating; instead, it is an indication that there was enhanced local subsidence. Based on the hypothesis that the

development of local sea breeze circulation regulates the local subsidence, we studied the timing of the development of sea breeze using the wind measurements at MAML. Sea breeze onset time was determined from wind shifts. The winds just prior to sea breeze onset were light and variable. As the surface heated the winds shifted and became steady from the west. The wind speed at this time was annotated along with the full development time. Our results show that the peak onset time was at 0800 and 0900 hours. This corresponds very well with the decrease of the BLH seen from the composite diurnal variation of the BLH. We then concluded that the sea breeze circulation sped up the cloud break up time through strengthening the subsidence velocity, resulting in a lower BLH.

To test the effects of surface flux and enhanced subsidence, a simple one dimensional moist mixed layer model was used to show the boundary layer and cloud evolution in response to these two types of forcing. The model was run using four cases. The first was a control case which held the surface flux and divergence constant. In case SFCflx, the divergence was held constant and the surface flux was allowed to vary as a sinusoidal function. This resulted in cloud break-up by 1400 each day. In case SBwk, the surface flux was allowed to vary in the same way as in SFCflx and the divergence was also allowed to increase slightly with time, the cloud break-up happened at 1230. Increasing the divergence with the largest rate (Case SBstrg) resulted in an even earlier breakup (1200). From the comparison of the vertical profiles of liquid water, temperature, and water vapor, we identified the strong warming of the boundary layer as a result of surface heat flux. Drying of the boundary layer is also evident as a result of enhanced turbulence and enhanced entrainment mixing. Essentially, the warming and drying of the boundary layer air effectively raised the lifting condensation level, resulting in gradual thinning of the cloud layer until its dissipation. The surface flux was found to have dominant effect on cloud break up, while the sea breeze subsidence modified the timing of the break up.

B. RECOMMENDATIONS

This study revealed the physical processes affecting the dissipation of stratocumulus cloud over the coastal land. It points to the dominant effects of increased

surface heat flux and enhanced subsidence that lead to cloud break up. The use of 1-dimensional model is helpful to reveal the direct connection between the cloud break up and the surface heat flux and subsidence, but it is highly simplified for a complex coastal region. Further examination of the measurements from other coastal sites should reveal the variation of the cloud break up characteristics along the coast. Simulation with a 3-D nonhydrostatic model, such as the Navy's COAMPS, should help explore the full interaction between the coastal dynamics and the cloud break up.

THIS PAGE INTENTIONALLY LEFT BLANK

LIST OF REFERENCES

ARM, 2005: ARM Instruments. Atmospheric Radiation Measurement Program (ARM). [Available from http://www.arm.gov/.] Date last accessed, March/2005

Banta, R. M., *L. D. Olivier*, and D. H. Levinson, 1993: Evolution of the Monterey Bay sea-breeze layer as observed by pulsed Doppler lidar. Journal of the Atmospheric Sciences, 50, 3959-3982.

Betts, A. K. 1990: Diurnal variation of California coastal stratocumulus from two days of boundary layer soundings. Tellus, 42A, 302-304pp.

Blaskovic, M., and R. Davis, 1991: Diurnal variation of marine stratocumulus over San Nicolas Island during July 1987. Mon. Wea. Rev., 119, 1469-1478pp.

Dorman, C.E., 1985: Evidence of Kelvin waves in California=s marine layer and related eddy generation. Mon. Wea. Rev., 113, 827-839.

Hanson, H.P., 1991: Marine stratocumulus climatologies. International J. of Climatology, 11, 147-164.

Lind, R., 2005: Class Notes: MR3455 Measurement Systems for the Marine and Coastal Atmospheric Boundary Layer, Naval Postgraduate School, Monterey, CA.

Neiburger, M., D.S. Johnson and C. Chien, 1961: Studies of the Structure of the Atmosphere over the Eastern Pacific Ocean in Summer. Vol. 1, University of California Publications in Meteorology, No. 1, 1-5.

NOAA, 2005: NOAA profiler Network. Forecast Systems Laboratory (FSL), National Oceanic and Atmospheric Administration (NOAA). [Available from http://www.profiler.noaa.gov/.] Date last accessed, March/2005

Nicholls, S., and J.D. Turton, 1986: An Observational Study of the Structure of Stratiform Cloud Sheets. Quart. J. R. Meteor. Soc., 112, 472, 461-480pp.

Ralph, F.M., P.J. Neiman and D. Reynolds, 1997: An Overview of Recent Applications of Wind Profiler and RASS Measurements in Mesoscale Meteorological Studies and Forecasting in the Western United States. COST-76, Profiler Workshop, 2-3pp.

Rogers, D.P., and D. Koracin, 1992: Radiative transfer and turbulence in the cloud-topped marine atmospheric boundary layer. J. Atmos. Sci., 49, 1473-1486.

Rodgers, C., 1976: Retrieval of Atmospheric Temperature and Composition from Remote Sounding Measurements of Thermal Radiation, *Rev.* Geophys. Space Phys., 14, 609– 624pp.

Stenger, S.A., 2004: Use of Wind Profilers for Mesoscale Analysis, Research Paper, Naval Postgraduate School, Monterey, CA 4-7pp.

Turton, J.D., and S. Nichols, 1987: A study of the diurnal variation of stratocumulus using a multiple mixed layer model. Quart. J. R. Meteor. Soc., 113, 969-1010pp.

Wang, Q., 2004: Class Notes: MR4414 Advanced Air-Sea Interaction. Modeling of Clear and Cloudy Boundary Layers, Naval Postgraduate School, Monterey, CA.

Wang, Q., D. L. Rosenberg and S. Wang 1999: Understanding the Processes of Stratocumulus Break-up in the Coastal Region, Research Paper, Naval Postgraduate School, Monterey, CA.

Whisenhant, M. K., 1999: Convection activities within the stratocumulus-topped boundary layer. M. S. Thesis, Naval Postgraduate School, Monterey, CA, 85pp.

INITIAL DISTRIBUTION LIST

1. Defense Technical Information Center
   Ft. Belvoir, Virginia

2. Dudley Knox Library
   Naval Postgraduate School
   Monterey, California

3. Chairman, Code 373
   Department of Meteorology
   Naval Postgraduate School
   Monterey, California

4. Professor Qing Wang, Code 373
   Department of Meteorology
   Naval Postgraduate School
   Monterey, California

5. Professor Wendell A. Nuss, Code 373
   Department of Meteorology
   Naval Postgraduate School
   Monterey, California

6. LCDR Matthew J. Moore
   Monterey, California